Quaternary Science Reviews 97 (2014) 102–120

Contents lists available at ScienceDirect

Quaternary Science Reviews

journal homepage: www.elsevier.com/locate/quascirev

East Antarctic deglaciation and the link to global cooling during the Quaternary: evidence from glacial geomorphology and ^{10}Be surface exposure dating of the Sør Rondane Mountains, Dronning Maud Land

Yusuke Suganuma [a, b, *], Hideki Miura [a, b], Albert Zondervan [c], Jun'ichi Okuno [a, d]

[a] National Institute of Polar Research, 10-3 Midoricho, Tachikawa, Tokyo 190-8518, Japan
[b] Department of Polar Science, School of Multidisciplinary Sciences, The Graduate University for Advanced Studies (SOKENDAI), Midori-cho 10-3, Tachikawa, Tokyo 190-8518, Japan
[c] GNS Science, National Isotope Centre, Lower Hutt 5010, New Zealand
[d] Japan Agency for Marine-Earth Science and Technology (JAMSTEC), 3173-25 Showa-machi, Kanazawa-ku, Yokohama, Kanagawa 236-0001, Japan

ARTICLE INFO

Article history:
Received 18 November 2013
Received in revised form
4 April 2014
Accepted 7 May 2014
Available online

Keywords:
Quaternary
East Antarctic Ice Sheet
Surface exposure dating
Beryllium-10
Glacial isostatic adjustment (GIA)
Southern Ocean

ABSTRACT

Reconstructing past variability of the Antarctic ice sheets is essential to understand their stability and to anticipate their contribution to sea level change as a result of future climate change. Recent studies have reported a significant decrease in thickness of the East Antarctic Ice Sheet (EAIS) during the last several million years. However, the geographical extent of this decrease and subsequent isostatic rebound remain uncertain. In this study, we reconstruct the magnitude and timing of ice sheet retreat at the Sør Rondane Mountains in Dronning Maud Land, East Antarctica, based on detailed geomorphological survey, cosmogenic exposure dating, and glacial isostatic adjustment modeling. Three distinct deglaciation phases are identified for this sector during the Quaternary, based on rock weathering and ^{10}Be surface exposure data. We estimate that the ice sheet thinned by at least 500 m during the Pleistocene. This thinning is attributed to the reorganization of Southern Ocean circulation associated with global cooling into the Pleistocene, which reduced the transport of moisture from the Southern Ocean to the interior of EAIS. The data also show that since the Last Glacial Maximum the ice surface has lowered less than ca 50 m and that this lowering probably started after ca 14 ka. This suggests that the EAIS in Dronning Maud Land is unlikely to have been a major contributor to postglacial sea-level rise and Meltwater pulse 1A.

1. Introduction

While it is broadly accepted that the Antarctic ice sheets play a major role in the Earth's global climatic system, many questions remain due to the multitude of processes and timescales involved. Climate models (e.g., DeConto and Pollard, 2003; Huber et al., 2004; Pollard and DeConto, 2009) suggest that the main triggering mechanism for Antarctic ice sheet stability is CO_2 concentration in the atmosphere. However, the response of the Antarctic cryosphere to contemporary increases in atmospheric CO_2 remains uncertain. Of particular relevance is the question of how much increase in global mean sea level should be expected from melting of Antarctic ice, under different future global climate scenarios (Bindoff et al., 2007). Reconstructing past variability (stability) of the Antarctic ice sheet will help with finding answers to these questions. At present, the evolution of the West Antarctic Ice Sheet (WAIS) and the larger East Antarctic Ice Sheet (EAIS) through the Neogene and Pleistocene, is not well understood. Recent studies have reported a significant decrease in thickness of the EAIS during the last several million years (e.g., Fogwill et al., 2004; Fink et al., 2006; Huang et al., 2008; Di Nicola et al., 2009, 2012; Strasky et al., 2009; Altmaier et al., 2010; Kong et al., 2010; Lilly et al., 2010; Liu et al., 2010). However, the geographical extent of this decrease and its response and feedback to the global climate remain uncertain. In addition, the nature of the glacio-eustatic rise following the Last Glacial Maximum (LGM), including the extremely rapid sea-level rise event "Meltwater pulse 1A (MWP-1A)", remains elusive (e.g.,

* Corresponding author. National Institute of Polar Research, 10-3 Midoricho, Tachikawa, Tokyo 190-8518, Japan. Tel.: +81 42 512 0702.
E-mail address: suganuma.yusuke@nipr.ac.jp (Y. Suganuma).

http://dx.doi.org/10.1016/j.quascirev.2014.05.007

Clark et al., 2002; Peltier, 2005; Mackintosh et al., 2013). The current lack of data from East Antarctica, especially Dronning Maud Land, makes it difficult to estimate the location(s) of melting ice responsible for this prominent feature of the last deglaciation.

In this study, we focus on the glacial history of the Sør Rondane Mountains in Dronning Maud Land, East Antarctica (Fig. 1). This mountain range provides rare isolated rock outcrops (nunataks) that are distant (ca 150 km inland) from coastal outlet glaciers. Also, there is geomorphological evidence that a large part of these mountains was covered by an expanded ice sheet (e.g., Van Autenboer, 1964; Iwata, 1987; Hirakawa et al., 1988; Aniya, 1989; Hayashi and Miura, 1989; Hirakawa and Moriwaki, 1990; Moriwaki et al., 1991). These facts make the Sør Rondane Mountains a valuable site to investigate elevation changes of the EAIS.

The glacial history of the Sør Rondane Mountains has in some sectors been reconstructed from tills and trimlines (Hirakawa et al., 1988; Moriwaki et al., 1992), using a weathering index (Moriwaki et al., 1991, 1994) and from cosmogenic exposure ages (^{10}Be and ^{26}Al: Nishiizumi et al., 1991, 1998; Matsuoka et al., 2006). Although these pioneering studies have contributed greatly to our understanding of the glacial history of these mountains, they can be improved by using modern methods and apparatus. The first issue is that elevations in previous studies were determined via astronomical positioning. Its level of accuracy is inadequate for the derivation of exposure ages from cosmogenic isotopes because their rates of in situ production strongly depend on atmospheric depth (e.g., Gosse and Phillips, 2001). Global positioning systems (GPS) provide the necessary level of accuracy. Secondary, the refinement of cosmogenic nuclide production scaling models since the late 1990s (e.g., Stone, 2000) was not considered in those previous studies. The more recent models reliably incorporate dependency on geomagnetic location and atmospheric depth (Gosse and Phillips, 2001). Thirdly, the sampling sites are now more carefully chosen and a more precise method is available for sampling rock surfaces (Suganuma et al., 2012). These method improvements help to minimize the impact of erosion and sample shape on cosmogenic exposure ages. The fourth issue is that isostatic rebound of the mountains, due to mass loss with decreasing ice sheet thickness, was not considered in past studies. Glacial isostatic adjustment (GIA) modeling enhances accuracy in estimating changes in thickness and volume of the EAIS (e.g., Lilly et al., 2010). In this study, we advance the research on the glacial history of the Sør Rondane Mountains by combining a new survey of local geomorphological features, with exposure dating of newly sampled rock surfaces using cosmogenic ^{10}Be and with GIA modeling.

2. Study area

The Sør Rondane Mountains emerge as a large group of nunataks covering an area of ca 2000 km^2 within Dronning Maud Land, East Antarctica (Fig. 1). The elevation of the ice sheet surface at the northern side of the Sør Rondane Mountains is about 1000 m, rising to 2500 m in the south. The mountains are mainly composed of low- to high-grade metamorphic rocks and various plutonic rocks that intruded into the metamorphic bedrock (e.g., Shiraishi et al., 1997). The time of the last tectonothermal event of the mountains has been estimated at 500–650 Ma based on sensitive high-resolution ion microprobe U–Pb zircon ages (Shiraishi et al., 2008). The absence of active structures and the lack of Cenozoic volcanism suggest that the Sør Rondane Mountains have been geologically stable over the last 500 Ma.

The current mean annual air temperature at Asuka Station (965 masl), located at the northern margin of the mountain, is −18.4 °C and in summer the air temperature rarely exceeds the freezing point (Matsuoka et al., 2006). Since the elevation of the ice sheet increases toward the south, most of the mountains are assumed to be below the freezing point permanently. It snows throughout the year, but the mountains are essentially snow-free in

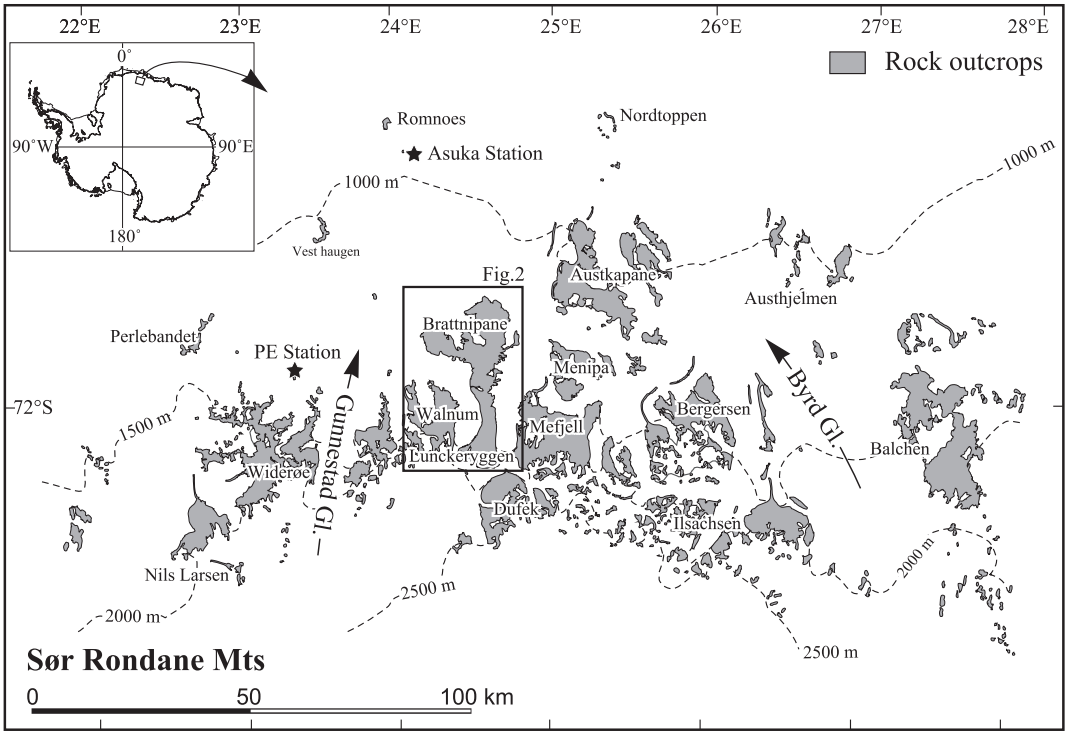

Fig. 1. Location and setting of the Sør Rondane Mountains. The box in the middle marks the location shown in Fig. 2. PE Station = Princess Elizabeth Station.

summer probably due to sublimation. This view is supported by Takahashi et al. (1992), who reported a large sublimation rate (200–280 mm y^{-1}) at the bare ice field near the Asuka station.

This study targets the Brattnipane, Lunckeryggen, and Walnumfjellet ranges located in the central part of the Sør Rondane Mountains (Fig. 2a). Depositional and erosional glacial landforms are found at various heights in this area, which makes it possible to reconstruct the past change of the EAIS thickness in the Dronning Maud Land sector. Many parts of the Brattnipane range are flat-topped ridges (Fig. 3a and b), with flanks that are mostly covered by thin tills (Fig. 3c). Glacial striations are observed on abraded surfaces at 2488 masl peak (10011202) at Walnumfjellet (Fig. 3d), and on the west flank (2031 masl; 09121401) of Mt. Tekubi at Brattnipane (Fig. 3e). The directions of the glacial striations at Walnumfjellet vary from N0°E to N30°E and their direction on the west flank of Mt. Tekubi is N30°E. These landforms are consistent with significant modification by an overriding ice sheet at some point in time. There are also several moraine fields fringing the mountain blocks at almost the same level as the present ice surface (Fig. 3f). Moraine ridges, distributed between the Oyayubi and Hitosashiyubi Ridges at the Brattnipane (Fig. 3g) and at the large moraine field, on the west side of Lunckeryggen (Fig. 4a), are parallel to the ice-margin, suggesting lateral accretion of glacial deposits associated with thinning of the ice stream.

3. Methods

A detailed geomorphological and glacial geological survey in the central part of the Sør Rondane Mountains was carried out during a December 2009–February 2010 field campaign. During this survey, we used Ski-doo to access the study area from a basecamp at the Princess Elizabeth Station (Fig. 1).

3.1. Classification of geomorphic surfaces

Spatial relationships between units of glacial deposits and the distribution of glacial erosional features were determined to draw a geomorphological map of the study area, using aerial photography and on-site rock weathering analysis. The latter technique is a powerful tool to identify periods of ice sheet advance and retreat (e.g., Moriwaki et al., 1991, 1994; White et al., 2009). In this study, such an analysis was carried out at 16 sites of flat-topped ridges, flanks, and large moraine fields at Brattnipane, Lunckeryggen, and Walnumfjellet. These sites were selected on the basis of lowest influence of local effects on weathering rates. Examples of such effects are mountain shading of the solar radiation and driven snow bank: solar radiation impacts on rock temperature regimes, moisture availability, and concomitant disintegration/decomposition (e.g., Hansen et al., 2013). The weathering characteristics of glacial deposits were classified using the Moriwaki method (Moriwaki

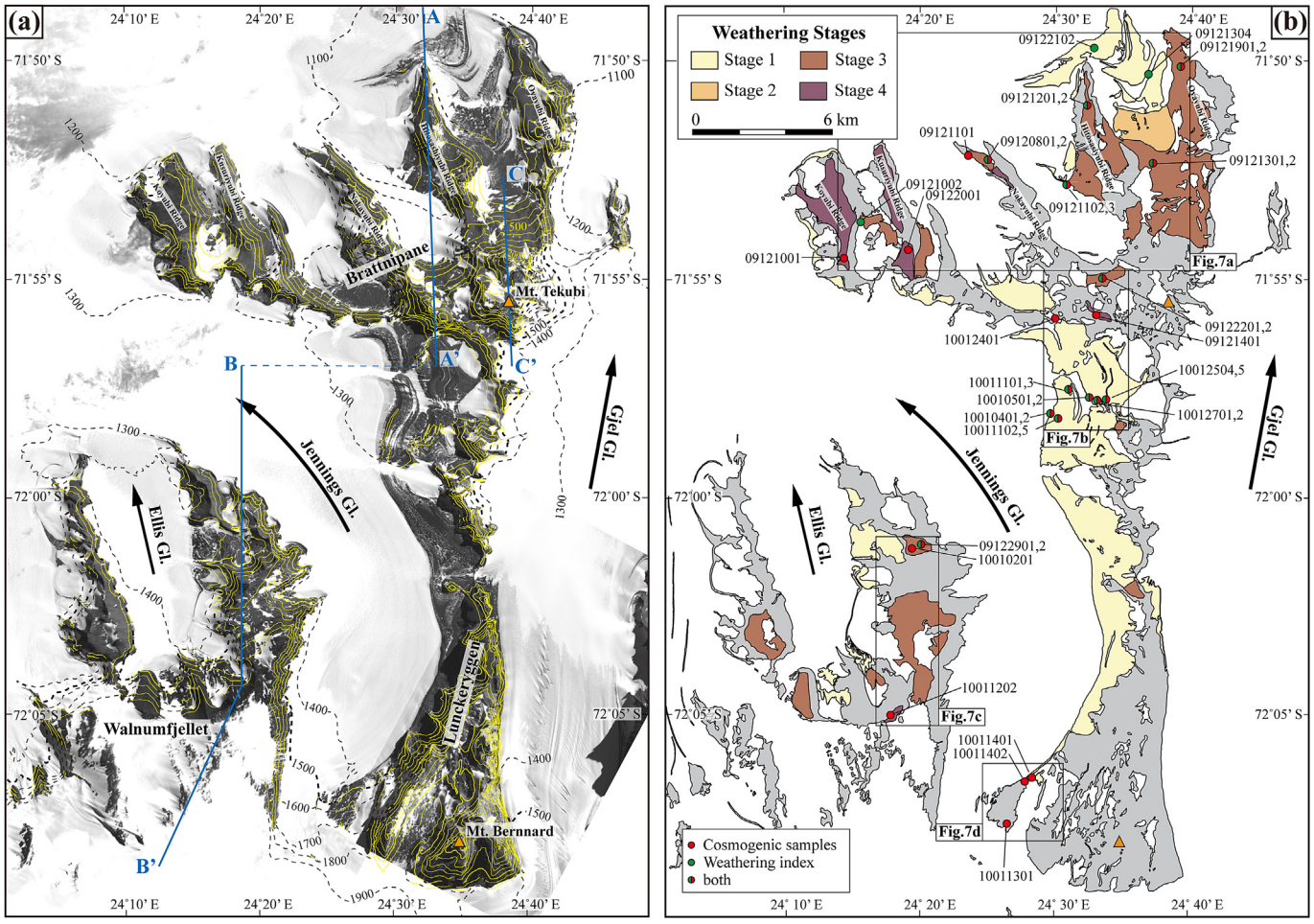

Fig. 2. Central part of the Sør Rondane Mountains (Brattnipane, Lunckeryggen, and Walnumfjellet): Satellite image ©JAXA (a) and geomorphologic interpretation (b). Transects A–A′, B–B′ and C–C′ in (a) are used to extract relief of the mountain chain in this area, to help interpret past changes in ice sheet thickness (Fig. 6). Small boxes in (b) correspond to Fig. 7a–d.

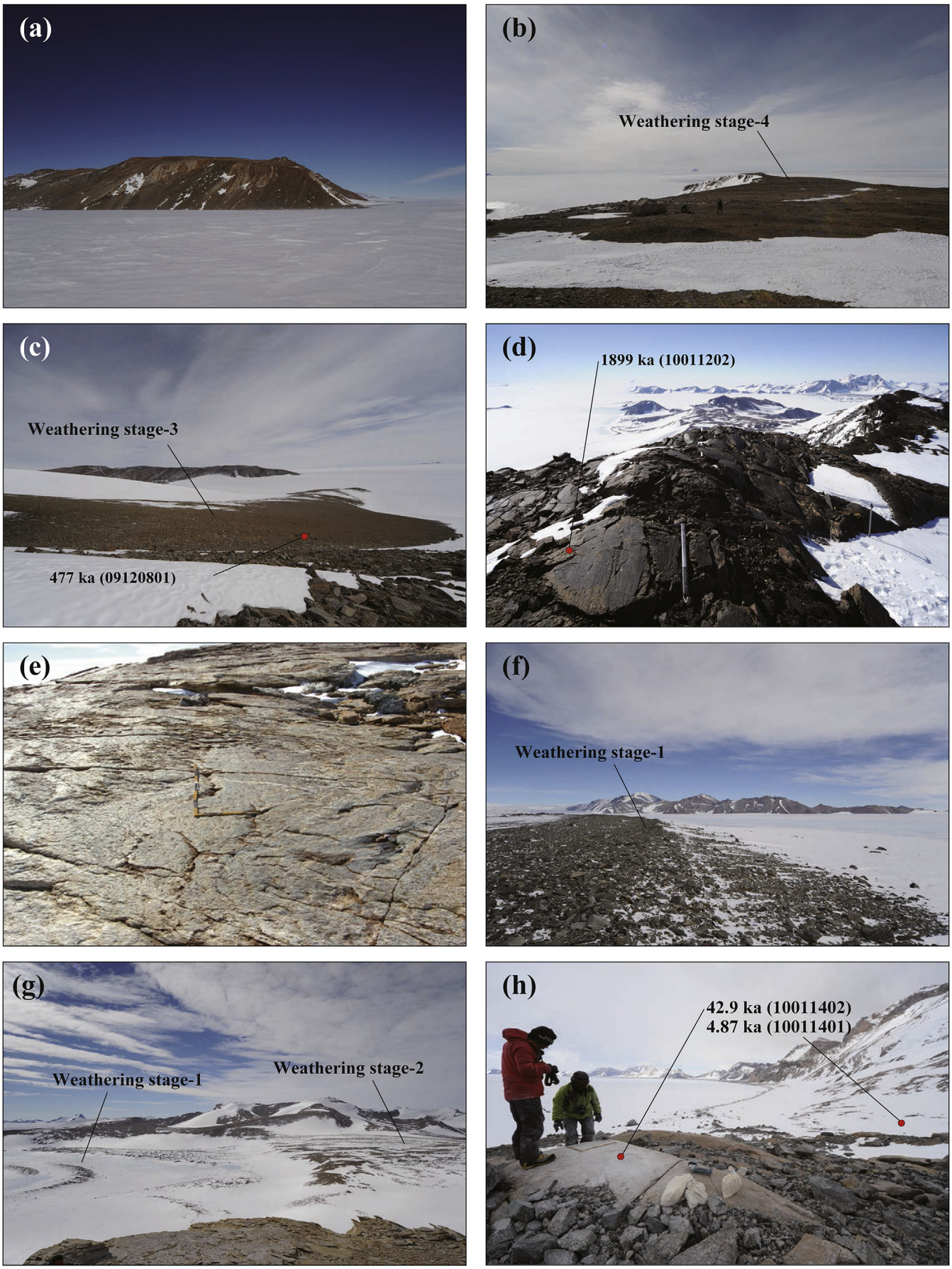

Fig. 3. Geomorphology and exposure ages of the Sør Rondane Mountains: (a) flat-topped Koyubi Ridge, Brattnipane; (b) flat-topped Kusuriyubi Ridge at Brattnipane; (c) glacial deposits on the flank at Nakayubi ridge; (d) glacial striations on an abraded surface at the 2488 masl peak (10011202) of Walnumfjellet; (e) glacial striations on an abraded surface at the west flank (2031 masl) (09121401) of Mt. Tekubi at Brattnipane; (f) a large moraine field at Lunckeryggen, almost at the same level as the present ice sheet level; (g) an overview of the moraine field between Oyayubi and Hitosashiyubi Ridges; and (h) a large rock outcrop at the SW edge of Lunckeryggen.

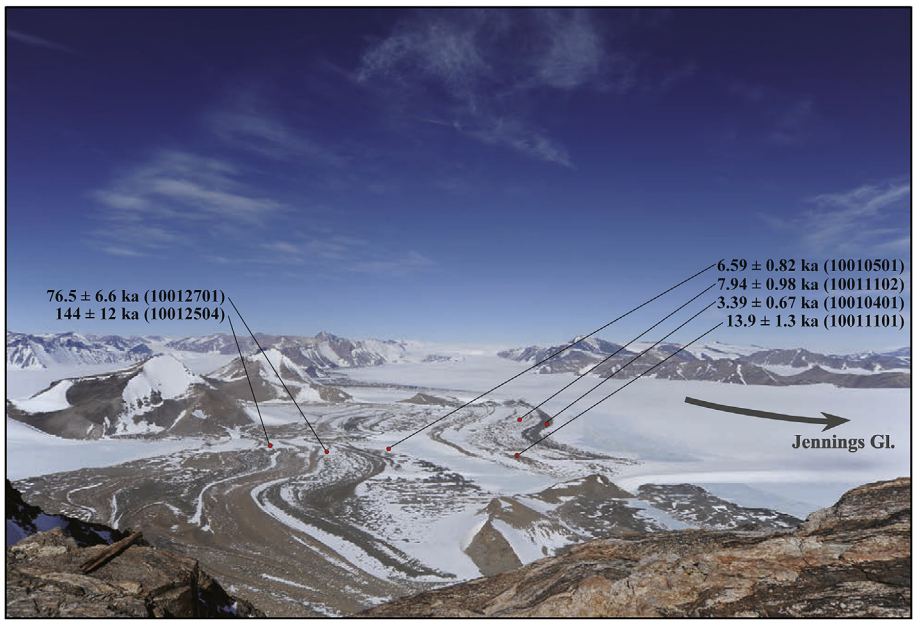

Fig. 4. Well-preserved, ice margin parallel moraine ridges at the large moraine field, west side of Lunckeryggen. The locations of sampling sites for cosmogenic dating are shown. The exposure ages indicate that the moraine ridges are stable after lateral accretion of the glacial deposits.

et al., 1991, 1994). It assigns the degree of weathering (DW) on the basis of (1) freshness and staining, (2) cavernous weathering, and (3) ventifact development of the largest 100 gravels in at $10 \times 10\ m^2$ surface of each till. Size and rock types of the gravels were also recorded. The method distinguishes five degrees of weathering:

DW 0 = a fresh clast, i.e., showing an original rock color without any weathered feature
DW 1 = a stained clast without cavernous weathering, ventifact and crumbling
DW 2 = a stained, cavernously weathered and/or wind-faceted, not crumbled clast
DW 3 = a distinctly stained and somewhat crumbled clast
DW 4 = a strongly stained and crumbled clast

The degree of weathering for the whole till, also called the Weathering Index (WI), is calculated by summing the number of individual gravels weighted by their respective DW values:

$$WI = 0 \times N_0 + 1 \times N_1 + 2 \times N_2 + 3 \times N_3 + 4 \times N_4, \quad (1a)$$

The WI scale is set by fixing the number of gravels in each WI determination:

$$N_0 + N_1 + N_2 + N_3 + N_4 = 100 \quad (1b)$$

Weathering characteristics of glacial deposits at each site are listed in Table 1. Based on the WI and field observation data, relative weathering stages of glacial deposits are classified, see Fig. 2b.

3.2. Surface exposure dating

Samples for surface exposure dating with cosmogenic ^{10}Be were collected from erratic boulders and glacially abraded bedrocks at various sites, see Figs. 3 and 4. The types of rock sample were granitoid and gneiss. In our sampling strategy, glacial geologic and geomorphologic settings of samples are of great importance. Lithology and size were carefully considered at each

Table 1
Geographical, weathering, and lithology details of the study area in the Sør Rondane Mountains. Weathering index (WI) is explained in Section 3.1. Ellip. height = ellipsoidal height.

Locality	Site	Lat. °S	Long. °E	Ellip. height (m)	Degree of weathering					WI	Lithology						
					0	1	2	3	4		Gn	To	Gr	Amp	And	Sy	uk
Brattnipene	09120802	71°52.14′	24°24.60′	1352	0	0	9	44	47	338	74	7	9	0	7	0	3
Brattnipene	09121002	71°53.48′	24°15.43′	1288	0	0	16	63	21	305	62	3	29	0	4	2	0
Brattnipene	09121103	71°52.93′	24°31.36′	1166	0	0	12	66	22	310	92	0	4	3	0	0	1
Brattnipene	09121202	71°50.90′	24°31.99′	1332	0	0	8	69	23	315	75	0	22	3	0	0	0
Brattnipene	09121302	71°52.23′	24°36.87′	1150	0	0	10	81	9	299	92	0	5	0	0	3	0
Brattnipene	09121304	71°50.17′	24°36.43′	1058	0	17	69	14	0	197	88	0	6	3	0	0	3
Brattnipene	09121902	71°49.99′	24°38.93′	1246	0	0	7	71	22	315	90	0	7	3	0	0	0
Brattnipene	09122102	71°49.65′	24°32.57′	1071	11	55	17	17	0	140	97	0	0	3	0	0	0
Brattnipene	09122202	71°54.88′	24°33.07′	1577	0	0	7	79	14	307	93	0	2	5	0	0	0
N.Lunckeryggen	10010402	71°58.02′	24°29.28′	1344	0	90	10	0	0	110	15	79	0	6	0	0	0
N.Lunckeryggen	10011105	71°57.48′	24°30.59′	1314	7	71	20	2	0	117	90	0	0	10	0	0	0
N.Lunckeryggen	10011103	71°58.11′	24°29.74′	1322	3	90	7	0	0	104	87	0	0	13	0	0	0
N.Lunckeryggen	10010502	71°57.63′	24°32.06′	1304	0	83	17	0	0	117	78	4	3	13	2	0	0
N.Lunckeryggen	10012702	71°57.70′	24°32.68′	1319	3	95	2	0	0	99	17	76	4	3	0	0	0
N.Lunckeryggen	10012505	71°57.72′	24°33.29′	1316	0	14	79	7	0	193	43	36	12	6	0	0	3
Walnumfjellet	09122902	72°01.01′	24°19.60′	1606	0	0	8	83	9	301	86	0	5	9	0	0	0

Table 2
Sample details pertinent to the derivation of ^{10}Be surface exposure ages. Surface erosion rates are estimated in Section 3.2. Correcting the ^{10}Be production rate for uplift by glacial isostatic adjustment (GIA) yields a more accurate estimation of ice sheet thickness. Ellip. height = ellipsoidal height.

Sample	Locality	Sample type	Lithology	Lat. °S	Long. °E	Ellip. height	Elevation (m)	Height above ice sheet (m)		Thickness (cm)
								Without GIA correction	With GIA correction	
10012401	Brattnipane	Erratic	Gneiss	71°55.81′	24°28.69′	1289	1271	20	20	2.5
09121301	Brattnipane	Erratic	Gneiss	71°52.23′	24°36.87′	1150	1132	100	40	3.0
09121201	Brattnipane	Erratic	Gneiss	71°50.90′	24°31.99′	1332	1314	119	60	2.0
09121102	Brattnipane	Erratic	Gneiss	71°52.93′	24°31.36′	1166	1148	−60	–	2.0
09120801	Brattnipane	Erratic	Gneiss	71°52.14′	24°24.60′	1352	1334	126	70	2.0
09122201	Brattnipane	Erratic	Gneiss	71°54.88′	24°33.07′	1577	1559	318	262	1.5
09121101	Brattnipane	Erratic	Granitoid	71°52.05′	24°23.15′	1246	1228	24	–	2.0
09121001	Brattnipane	Basement	Gneiss	71°54.40′	24°13.91′	1717	1699	475	344	2.0
09121401	Brattnipane	Basement	Gneiss	71°55.73′	24°32.62′	2031	2013	728	522	2.0
09121901	Brattnipane	Erratic	Gneiss	71°49.99′	24°38.93′	1246	1228	50	–	2.0
09122001	Brattnipane	Basement	Gneiss	71°54.22′	24°18.69′	1632	1614	390	–	1.5
10010401	N. Lunckeryggen	Erratic	Granitoid	71°58.02′	24°29.28′	1344	1326	44	44	2.0
10011102	N. Lunckeryggen	Erratic	Gneiss	71°58.11′	24°29.74′	1314	1296	14	14	2.5
10011101	N. Lunckeryggen	Erratic	Gneiss	71°57.48′	24°30.59′	1322	1304	22	22	2.5
10010501	N. Lunckeryggen	Erratic	Gneiss	71°57.63′	24°32.06′	1304	1286	4	4	2.0
10012701	N. Lunckeryggen	Erratic	Granitoid	71°57.70′	24°32.68′	1319	1301	19	19	2.5
10012504	N. Lunckeryggen	Erratic	Granitoid	71°57.72′	24°33.29′	1316	1298	16	16	2.5
10011401	S. Lunckeryggen	Basement	Granitoid	72°6.39′	24°27.81′	1423	1404	23	23	2.0
10011402	S. Lunckeryggen	Basement	Granitoid	72°6.44′	24°27.29′	1454	1435	54	54	2.0
10011301	S. Lunckeryggen	Basement	Granitoid	72°7.47′	24°25.98′	1747	1728	187	131	2.0
09122901	Walnumfjellet	Erratic	Gneiss	72°01.01′	24°19.60′	1606	1587	227	175	2.0
10010201	Walnumfjellet	Erratic	Gneiss	72°01.08′	24°18.93′	1567	1548	188	140	2.5
10011202	Walnumfjellet	Basement	Granitoid	72°04.95′	24°17.26′	2489	2470	1028	897	2.0

locality to identify rock surfaces most suitable for exposure dating. When selecting erratic boulders, two geometrical criteria were applied to minimize the likelihood of post-depositional overturning: size and orientation. Boulders should be as large as possible and their longest axis should be (near-) parallel to the ground surface.

In addition, we selected surfaces where field evidence suggests they must have eroded only slowly. For example, the glacial striations and/or preservation of the glacially polished surfaces are thought to be evidence of slow erosion. Uniform staining is also an indication that the surface was not eroded heterogeneously. Using an electric powered diamond saw (Suganuma et al., 2012), samples were taken from the tops of boulders to minimize shielding and as far from the edge as possible to avoid suppression of cosmogenic nuclide production due to neutron escape (Masarik and Wieler, 2003). The elevations of these samples were determined via handheld GPS and corrected to geoid heights at 71°55.00′S, 24°30.00′E for Brattnipane and northern half of Lunckeryggen, and at 72°05.00′S, 24°20.00′E for Walnumfjellet and the southern half of Lunckeryggen based on the Earth Gravitational Model 2008 (Pavlis et al., 2012). Sample details are listed in Table 2 and photographs of all sampling sites are shown in Fig. 1 of the Supplement.

The ^{10}Be sample preparation was performed at the University of Canterbury (Child et al., 2000; Mifsud et al., 2013). First, the rock samples were ground and sieved to 125–500 μm. Then, chemical cleaning using hot phosphoric acid was applied to dissolve non-quartz minerals and weak hydrofluoric acid to remove meteoric ^{10}Be from the surface of quartz grains. Prior to dissolution of the purified quartz with concentrated hydrofluoric acid, samples were weighed and beryllium carrier (0.26–0.56 mg Be) was added. Ion-exchange chemistry was then applied to separate beryllium from abundant metals in quartz such as Fe and Ti. The beryllium hydroxide was converted in quartz vials to the oxide form using a muffle furnace. Four chemistry blanks were prepared.

The ^{10}Be AMS measurements were performed with the eXtended Carbon Accelerator Mass Spectrometry system (XCAMS) at GNS Science, New Zealand. The sample BeO was mixed with roughly equal volume Ag powder inside the quartz vial and then transferred and pressed into copper cathode holders. A 40-position copper wheel was used to introduce the samples to the sputter ion source. Suppression of the stable isobar ^{10}B was accomplished with the differential energy-loss technique using a 50 nm thick Si-nitride foil on the high-energy side of the accelerator mass spectrometer and event gating in the energy spectrum from the particle detector (Müller et al., 2010). The measured ^{10}Be/^{9}Be ratios were normalized using NIST reference material SRM4325 with an assumed isotope ratio of ^{10}Be/^{9}Be = 2.79 × 10^{-11} atom atom^{-1} (Balco et al., 2008). The system's ability to measure ^{10}Be/^{9}Be ratios much lower than that was determined with a blank with ^{10}Be/^{9}Be ≈ 2 × 10^{-16} atom atom^{-1} determined with the CAMS facility at LLNL, USA (Rood et al., 2013). On XCAMS, this blank had an isotope ratio of ^{10}Be/^{9}Be = 5 × 10^{-15} atom atom^{-1}. This machine blank is one order of magnitude below the lowest ^{10}Be/^{9}Be ratio of all samples in this study, including the chemical processing blanks.

After correction for the machine blank, by subtracting it from ^{10}Be/^{9}Be values of the other cathodes in the wheel, the resulting values were converted to number of ^{10}Be atoms in the sample. For the four chemical processing blanks, the mean value and standard deviation were (1.7 ± 0.4) × 10^{6} ^{10}Be atoms. After subtracting this chemistry blank, net amounts of ^{10}Be atoms were converted to concentration values in quartz and subsequently to exposure ages using version 2.2 of the CRONUS on-line calculator (Balco et al., 2008), see Table 2. We chose the time-varying production rate model using Lal's geographical scaling method (Lal, 1991), later modified to better handle the special air pressure conditions of Antarctica (Stone, 2000). Correction factors for topographic shielding and surface dip were calculated after Dunne et al. (1999) and for sample thickness after Gosse and Phillips (2001) assuming a

Geometric shielding	Quartz diss. (g)	^{10}Be (10^6 atom/g)	^{10}Be age (ka) with no uplift no erosion	^{10}Be age (ka) with no uplift with erosion	Total uncertainty		^{10}Be age (ka) with uplift first run	Total uncertainty		^{10}Be age (ka) with uplift second run	Total uncertainty	
					+	−		+	−		+	−
0.990	69.09	0.93 ± 0.02	53.0	53.2	4.7	4.7	53.6	4.7	4.7	53.6	4.7	4.7
0.994	54.00	2.48 ± 0.02	163	165	15	15	170	15	15	170	15	15
0.999	78.40	3.47 ± 0.02	195	198	18	18	204	18	18	204	18	18
0.997	91.14	6.17 ± 0.03	421	433	42	42	453	42	42	454	42	42
0.992	59.81	7.47 ± 0.04	442	456	45	45	477	45	45	477	45	45
0.987	40.10	9.45 ± 0.06	472	487	49	49	509	49	49	510	49	49
0.998	67.59	14.74 ± 0.07	1104	1136	137	136	1203	138	137	1205	138	137
1.000	78.61	26.55 ± 0.08	1491	1706	274	270	1861	287	278	1858	286	277
0.997	88.51	40.93 ± 0.10	2072	2098	317	317	2329	318	318	2319	318	318
0.998	57.74	20.85 ± 0.13	1833	2207	444	429	2574	515	465	2560	513	464
1.000	45.98	33.30 ± 0.11	2411	3303	1153	1010	4593	–	1342	4549	–	1326
1.000	54.54	0.06 ± 0.01	3.39	3.39	0.67	0.67	3.39	0.67	0.67	3.39	0.67	0.67
0.999	65.28	0.14 ± 0.01	7.93	7.93	0.98	0.98	7.94	0.98	0.98	7.94	0.98	0.98
0.999	75.77	0.26 ± 0.01	13.9	13.9	1.3	1.3	13.9	1.3	1.3	13.9	1.3	1.3
0.999	18.32	0.12 ± 0.01	6.49	6.49	0.82	0.82	6.50	0.82	0.82	6.50	0.82	0.82
0.999	66.88	1.36 ± 0.01	75.4	75.5	6.6	6.6	76.5	6.6	6.6	76.5	6.6	6.6
0.997	69.86	2.47 ± 0.02	140	140	12	12	144	12	12	144	12	12
0.980	46.41	0.10 ± 0.01	4.80	4.87	0.82	0.82	4.87	0.82	0.82	4.87	0.82	0.82
0.985	89.71	0.85 ± 0.01	42.0	42.6	3.7	3.7	42.9	3.7	3.7	42.9	3.7	3.7
0.995	38.66	11.50 ± 0.06	507	513	50	50	535	50	50	535	50	50
0.980	99.53	15.49 ± 0.06	833	887	102	102	934	102	102	936	102	102
0.988	79.65	18.43 ± 0.06	1077	1173	151	150	1244	152	151	1246	153	151
0.999	12.06	50.77 ± 0.20	1755	1772	244	243	1902	244	244	1899	244	244

rock density of 2.65 g cm^{-3}. The CRONUS calculator incorporates these correction factors in the derivation of exposure ages from ^{10}Be concentrations.

When using a single cosmogenic isotope to determine the exposure age of a rock surface, an average rate of erosion for the exposure duration must be assumed (Gosse and Phillips, 2001). Minimum exposure ages are the direct result of the zero erosion assumption, and a (time-averaged) erosion rate co-determines by how much an actual exposure age exceeds its minimum. Exceptionally low erosion rates have been observed in many places in Antarctica. For example, Matsuoka et al. (2006) reported a 2.16 Ma exposure age for the abraded surface of the Walnumfjellet with an almost negligible erosion rate (<0.13 m Ma^{-1}) using ^{10}Be and ^{26}Al. They offer the explanations that the high elevation minimizes melting and sublimation of ice in the exposed rock and that an isolated mountain ridge is also unfavorable for receiving sand or snow particles that drive wind abrasion (Matsuoka et al., 2006). Similarly, low erosion rates were also obtained in other parts of Antarctica, including the Dry Valleys (e.g., Brook et al., 1995; Ivy-Ochs et al., 1995; Summerfield et al., 1999) and Shackleton Range (e.g., Fogwill et al., 2004). These data suggest that, during the Quaternary, high-elevation rock surfaces were relatively stable. Unfortunately, we could not obtain ^{26}Al data of sufficient quality due to a lack of quality control in preparing sub-samples for ^{27}Al analysis. Therefore, we proceed with estimating erosion by using these earlier studies and on the basis of differentiation by rock type and geomorphological features.

Two samples, found at sites 09121401 and 10011202, show glacial striations on their surface. Obviously, this signature of extreme low erosion is useful in keeping to a minimum the component in the ^{10}Be exposure age uncertainty that is due to erosion uncertainty. For these two samples with striations, we adopt 0–1 cm Ma^{-1} as the range of likely erosion rates. The remaining samples are grouped by rock type: granitoid and gneiss. Because of their silica surfaces, they too probably have eroded slowly, but no glacial striations are seen at these sampling sites. We adopt reported values for the same type of rocks in East Antarctica: 5–10 cm Ma^{-1} for gneiss (Huang et al., 2008) and 0–5 cm Ma^{-1} for granitoid (Di Nicola et al., 2012). We use these three ranges to fix an erosion rate of each group at their mid-point and we assume that these ranges represent 68% probably confidence intervals which can then be used for propagation of errors to (1-sigma) uncertainties of final ^{10}Be exposure ages. While failing to exclude the non-physicality of negative erosion, this assumption of normally (Gaussian) distributed erosion rate errors allows one to proceed with error propagation in the standard way (Hughes and Hase, 2010).

We have no quantitative information about snow cover at the Sør Rondane Mountains, but we assume that a mean surface snow mass balance of +111 mm y^{-1} for the Asuka drainage basin (Figs. 3-1 and 3-8 in National Institute of Polar Research (1997)) is a reasonable estimate for our study site. Most areas of the Sør Rondane Mountains are snow-free in summer. From that we infer that the low albedo of the nunataks promotes the complete removal of small amounts of accumulated snow through sublimation and/or ablation. Therefore, it seems plausible that time-averaged thicknesses of overlying snow/ice were at least one order of magnitude less than the attenuation length of fast neutrons ($\Lambda \approx 150$ g cm^{-2} = 150 cm in water/ice) and that a zero correction for attenuation by surface coverage is justified.

Below 2000 masl, the in situ ^{10}Be production rate increases by ca (7–10)% *per* 100 m higher elevation (Balco et al., 2008). If sample sites have experienced significant uplift during their exposure, presumably due to crustal uplift following ice sheet retreat, then this response needs to be incorporated in the calculation of sample exposure ages. In theory, collinearity between production rates,

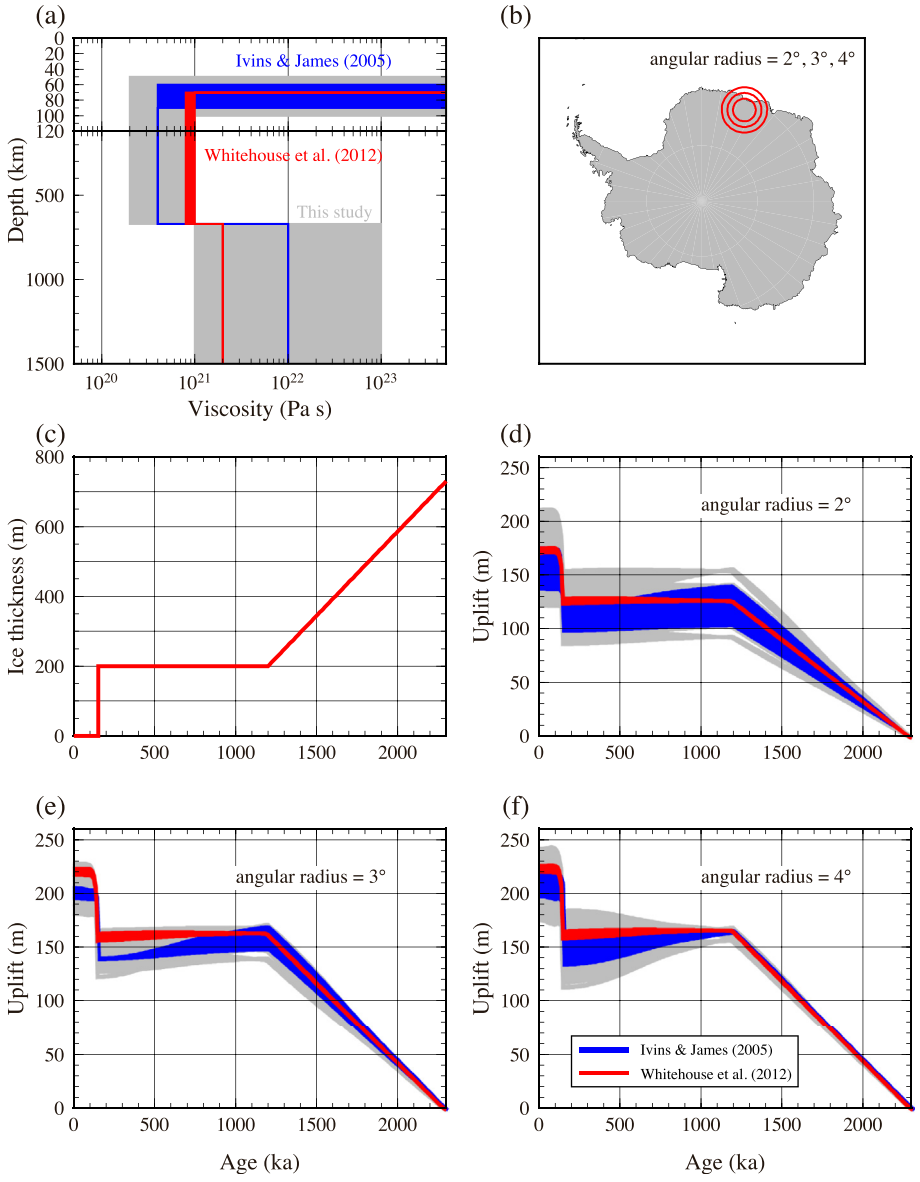

Fig. 5. GIA modeling results of the second iteration for the Sør Rondane Mountains. (a) Mantle viscosity profiles, including the lithospheric thickness used in this study. The blue and red profiles are taken from Ivins and James (2005) and Whitehouse et al. (2012), respectively. The gray viscosity profile has been used in this study and was obtained by analysis of relative sea-levels in the world and satellite geodetic observations (e.g., Lambeck and Chappell, 2001; Argus and Peltier, 2010). (b) Disks with different radius in the GIA model calculation. The three disks are centered at the Sør Rondane Mountains. (c) Ice sheet elevation change deduced from exposure ages. Uplift histories since 2.3 Ma resulting from the GIA model calculation are shown for three disk load radii: 2° (d), 3° (e), and 4° (f). (For interpretation of the references to colour in this figure legend, the reader is referred to the web version of this article.)

exposure ages, uplift and reconstructed elevations could lead to an underdetermined system of observations, derived parameters, and corrections. A possibly complicating factor is that, at present, calculations for exposure ages and uplift can't be made simultaneously. Convergence to a stable set of ages and uplift history needs to be confirmed by iterating between these two types of calculations.

3.3. Glacial isostatic adjustment modeling

Accuracy in estimating thickness changes of ice sheets can be improved by accounting for isostatic rebound of the solid Earth due to changes in ice loading. We use the glacial isostatic adjustment (GIA) model described by Nakada and Lambeck (1987) to calculate the ice load term for the EAIS. Here, we summarize the components of this model and justify our choice of key parameter values.

In the GIA model, the Earth is represented by a spherically symmetric, self-gravitating Maxwell body comprising an elastic lithosphere, an upper and lower mantle. The upper and lower mantle are defined to be uniform-viscosity layers extending to the discontinuity at 660 km depth and the core–mantle boundary at 2900 km depth, respectively. The elasticity and density structure are derived from the Preliminary Earth Reference Model (Dziewonski and Anderson, 1981). Plausible ranges within which we varied lithosphere thickness, upper and lower were: 50–100 km, (1–10) $\times$ 10^{20} Pa s, and (1–100) $\times$ 10^{21} Pa s, respectively. The corresponding viscosity profile is compared in Fig. 5a with profiles derived from Late Pleistocene and Holocene relative sea-level changes and space geodetic observations (e.g., Lambeck and Chappell, 2001; Ivins and James, 2005; Argus and Peltier, 2010; Whitehouse et al., 2012). Because of the large degree of overlap with these other viscosity profiles, our model behaves in a

manner that consistent with global sea-level change over the past 20 ka.

In this study, we adopt the single-disk model to estimate the effective total uplift induced by ice sheet thinning at the Sør Rondane Mountains. Simulating the effect of crustal rebound was done for disk areas of three different radii: angular distance = 2°, 3° and 4° (Fig. 5b). Because GIA calculation based on the Earth models with 70–100 km of elastic thickness, requires an ice model resolution of 1–2° disk radius (e.g., Nakada and Lambeck, 1987), we regard the 2° disk radius as the minimum size. At the same time, we assume the maximum radius of 4° for this modeling to represent the largest ice sheet coverage restricted by the continental shelf break.

We repeat the sequence of GIA modeling and exposure age calculation process, because the recalculated exposure ages changes the history of ice sheet's elevation, which, in turn, changes the amount of isostatic rebound. We assume that the ice thickness is uniform across the disk and starts to vary in time at 2.1 Ma for the first iteration (S. Fig. 2c) and at 2.3 Ma for the second iteration (Fig. 5c), based on the exposure ages to be presented in Section 4.2. The results from these ice load models and the viscosity profiles (Fig. 5d–f) for the area under study and the interaction with the ^{10}Be exposure determinations will be discussed in Section 5.

4. Results

4.1. Weathering stages

To quantify the weathering characteristics of glacial deposits, their degree of weathering was determined with the Moriwaki classification method presented in Section 3.1. Fig. 6a shows, for each rock type at each site, the number of gravels versus weathering degree (DW). Using these data in a scatterplot of average DW values versus weathering index (WI) (Fig. 6b), we see a clear correlation between these parameters. This suggests that differences in weathering throughout all studied sites show no dependence on rock type. This supports our approach to apply this method across all deposits in this study.

The weathering characteristics of glacial till deposits in some part of the Sør Rondane Mountains have been studied before (Moriwaki et al., 1991, 1994). They adapted five weathering stages (1a, 1b, 2, 3, 4) for the glacial deposits with one preceding stage 5 for the oldest glacial event. Although they subdivided the youngest weathering stage 1 into stages 1a and 1b based on a slight difference in WI values, they lack clear segregation in terms of elevation and geomorphological features. For our study, we regard sub-stages 1a and 1b as one stage 1. In addition, weathering stage 5 was used by Moriwaki et al. (1991, 1994) for abraded surfaces, rather than for glacial deposits, as evidence of the oldest glacial event. However, we see no reason to make a distinction between weathering stages 4 and 5 and we therefore consolidate them into one stage 4. We discuss this later in more detail in Section 4.1.3.

4.1.1. Stages 1 and 2

Weathering stage 1 is distributed around the moraine field fringing the mountain blocks within ±30 m elevation from the present ice surface level (Figs. 2b, 3e and f). Glacial deposits of this stage are fresh or relatively fresh. Boulders in these deposits have no or little iron staining, are largely intact, and often have their glacial polish and striations still preserved. A few boulders displaying tafoni are found inside the moraine field. These rare, strongly weathered erratics probably originate from recycling during later advances of the ice sheet. Moriwaki index values for deposits of this stage are low (WI = 99–193), generally increasing toward the inside of the moraine field. Some parts of the moraines associated with these deposits are ice-cored. These features indicate that the ice sheet margin widened by up to ca 3 km at the large moraine field at Lunckeryggen and up to ca 3.5 km between Oyayubi Ridge and Hitosashiyubi Ridge at Brattnipane, followed by ice stream thinning and accretion of glacial deposits. This stage 1 corresponds to stages 1a and 1b of Moriwaki et al. (1991, 1994).

Glacial deposits corresponding to stage 2 are distributed between Oyayubi and Hitosashiyubi Ridges at Brattnipane, and are moderately weathered (Fig. 2b). These glacial deposits are found slightly higher than stage 1 (Fig. 3f), suggesting that they were formed when the ice sheet level was slightly higher than present. Unfortunately, fieldwork logistics limited the collection of sufficient information to construct Moriwaki index for this stage.

4.1.2. Stage 3

Stage 3 is characterized by strongly weathered glacial deposits, displaying extensive tafoni or wind faceting. Their Moriwaki index values range from WI = 299 to 338. These glacial deposits are distributed around the flank of the flat-topped ridges and contain large erratic boulders. U-shaped valleys have developed between the Oyayubi and Hitosashiyubi Ridges at Brattnipane and Walnumfjellet (Figs. 2b and 3c). No glacial deposits with low degrees of weathering were found in this stage. Taken together, these facts strongly suggest past glacial erosion and retreat at the Sør Rondane Mountains.

4.1.3. Stage 4

The flat-topped ridges of the Brattnipane have been assigned weathering stage 4 by Moriwaki et al. (1991, 1994), based on the most heavily weathered glacial deposits from the terrace of the Hitosashiyubi Ridge. We, however, find that the deposits on the flat-topped ridges are composed of bedrock mostly, plus a few erratics, and we therefore do not assign them a Moriwaki index. Abraded surfaces with glacial striations are found at the 2489 m peak (10011202) on Walnumfjellet (Fig. 3d) and at the west flank (2031 m) (09121401) of Mt. Tekubi, Brattnipane. This indicates that the glacial landform was made by an ancient overriding ice sheet, with glacial deposits either subsequently removed from the landform or sparsely deposited originally. Weathering stage 4 appears to be associated with a glacial advance that covered most of the Sør Rondane Mountains and is responsible for the present-day landforms with flat-topped ridges and abraded surfaces.

4.2. Surface exposure dates without GIA correction

In total, 23 ^{10}Be exposure ages were obtained for rock surfaces at 1150–2489 masl in the central part of the Sør Rondane Mountains (Fig. 2b). All relevant sample data from the ^{10}Be analysis are found in Table 2. The exposure ages are distributed over a wide range, 3.34–3160 ka. Best estimates of erosion rates were given in Section 3.2 and no further information is available to better constrain them. But, even though we chose erosion rate uncertainties in a simplified and conservative way, their contribution to final age uncertainties is, for all samples except one, less than that from uncertainty in the scaling model that we applied.

The exception is sample 09122001. The relative size of its error components warrants some discussion as it clearly illustrates the limitation to our application of the 'single isotope' method. In general, as a sample's ^{10}Be concentration gets closer to its secular equilibrium value, where cosmogenic production is balanced by radiometric decay and erosion, the exposure age becomes less well determined. Also, analytical errors and uncertainties in the scaling models and erosion rate assumptions can, depending on their size, show the inherent non-linear nature of the relation between ^{10}Be concentration and exposure age, resulting in asymmetric errors. Sample 09122001 is exemplary of this. There is no doubt that it has

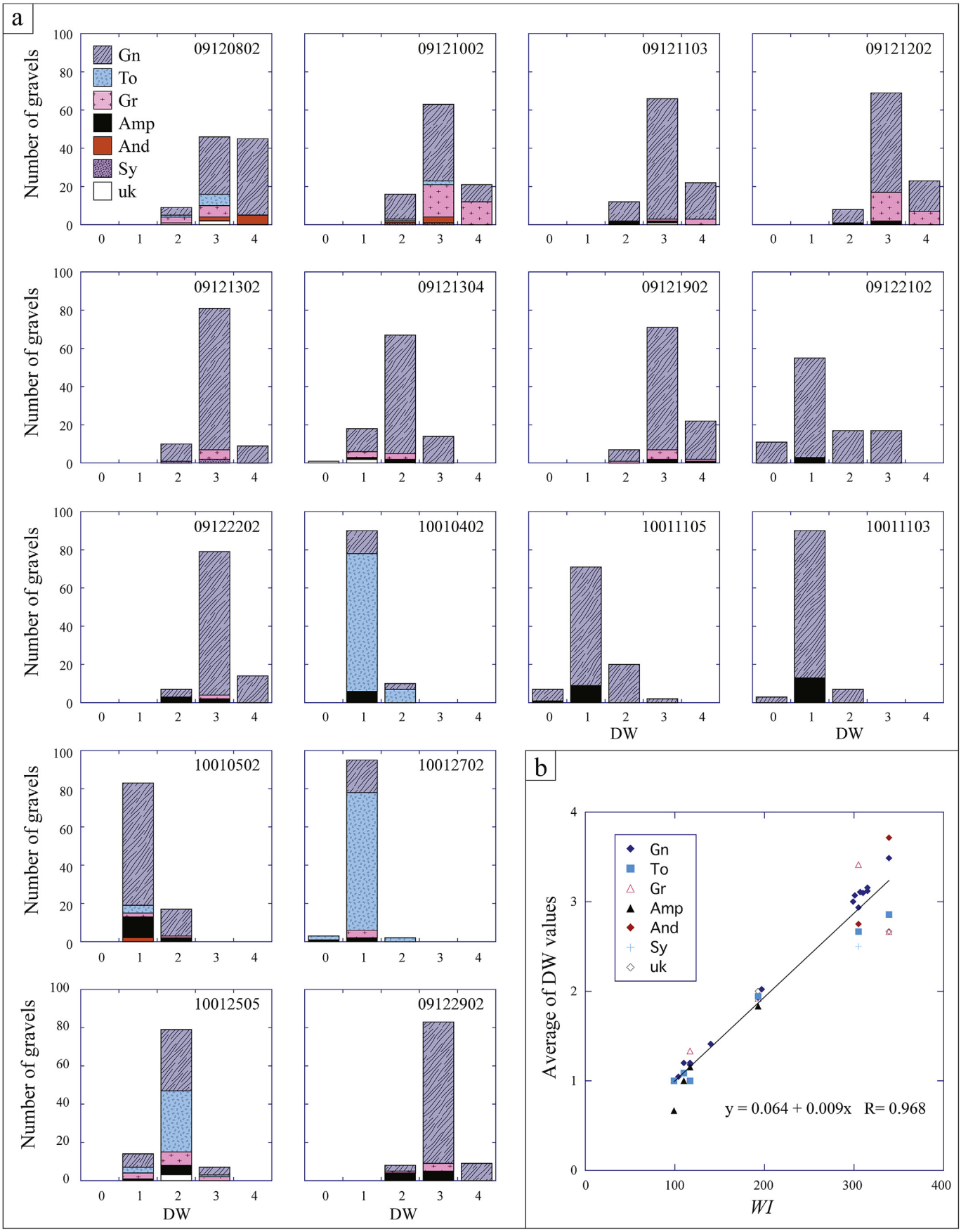

Fig. 6. (a) Degree of weathering (DW) versus number of gravels for each rock type. (b) Average of the DW values for each rock type versus WI at each site. Abbreviations: Gn, Gneiss; To, Tonalite; Gr, Granitoid; Amp, Amphibole; And, Andesite; Sy, Syenite; uk, unknown.

been exposed for several Ma, but the lack of knowledge about its actual rate of erosion renders its age poorly determined. From an assumed erosion rate of 7.5 cm Ma^{-1} and after correction for uplift we derive a best-estimate exposure age of 4.5 Ma. While the uncertainty interval on the negative side is finite (1.3 Ma), the age uncertainty interval on the positive side extends to infinity. This exposure age would be the oldest of our data set and the only result consistent with exposure starting before the Pleistocene. On the other hand, if we assume this rock eroded less than our best estimate by only $^1/_3$ (i.e. 5 cm Ma^{-1}), a possibility we can't exclude on the basis of rock type and geomorphological features, then we obtain not only a significantly younger age but also a much less imprecise result: 3.6 ± 1.1 Ma. While sample 09122001 clearly shows the limits of our approach, the situation for the remainder of the data set is much better: secular equilibrium concentrations are not reached and confidence intervals on the exposure ages are nearly symmetric and small enough to render the ages meaningful.

The ^{10}Be exposure ages are generally increasing with elevation. However, some of the samples deviate from a general trend of decreasing exposure ages with decreasing elevation. In the remainder of Section 4.2, we consider the spatial distribution of exposure ages in order to identify outliers. The correction for uplift is addressed in Section 5.

4.2.1. Brattnipane

The eight samples from the northern part of the Brattnipane that are in the age range 162–3160 ka are located at elevations of 1150–1717 masl (Fig. 7a). Their exposure ages correlate well with their weathering stage assignments 3 and 4. Samples 09121001 and 09122001 are from weathering stage 4 and located on top of Koyubi and Kusuriyubi ridges, respectively (Fig. 2b). The exposure age of sample 09121001 is 1670 ka. Although the weathering of glacially abraded bedrock at this site seems to be very weak (S. Fig. 1b), no glacial striations are visible. In contrast, sample 09122001 was taken from relatively weathered bedrock at 1632 masl (Supp. Fig. 1c). The ^{10}Be exposure age of this site is 3160 ka, which is the oldest exposure age in this study. Although the distance between these two samples is only ca 2.8 km and their altitude difference is only ca 90 m, sample 09122001 has been exposed almost twice as long as sample 09121001.

Sample 09122001 does not fit the general trend of decreasing exposure ages with decreasing elevation. To resolve this anomaly, we follow the practice of others where younger ages are considered to be more representative of the duration of exposure of the rock surface and the oldest ages are considered to be the result of complex exposure histories under cold-based, non-erosive ice sheets (e.g. Stone et al., 2003; Balco, 2011). Evidence from a paired nuclide such as ^{26}Al would allow to (dis)prove this interpretation. Despite the fact no such information is available, we regard sample 09122001 to be an outlier.

Similarly, samples 09121901 and 09121101 from weathering stage 3 show older exposure ages than those of other samples from that stage. Their elevations appear to be lower than the general trend of decreasing exposure ages with decreasing elevation. Stated differently: given their elevation and degree of weathering, we would have expected much younger exposure ages than actually observed. This suggests that these erratic rocks were recycled during fluctuation of the ice sheet thickness. Sample 09121102 is from a deeper part of the moraine field fringing between the Hitosashiyubi and Nakayubi ridges, suggesting this area became isolated during an earlier stage of ice sheet thinning. In order to avoid the discussion that follows being influenced too much by apparent outliers and local effects, samples 09122001, 09121901, 09121101, and 09121102 are now excluded.

4.2.2. Flank of Mt. Tekubi and the large moraine field at Lunckeryggen

The nine samples from the flank of Mt. Tekubi and the large moraine field at Lunckeryggen fall in the age range 3.34–2050 ka and have elevations in the range 1289–2031 masl (Fig. 7b). Sample 09121401 from weathering stage 4 is located on top of the abraded surfaces at the west flank (2031 masl) of Mt. Tekubi, one of the highest elevation places studied. The glacial striations on these abraded surfaces (Supp. Fig. 1b) show that the present-day surface was glacially polished and not eroded since the last deglaciation. The exposure age estimate from ^{10}Be for the site is 2050 ka.

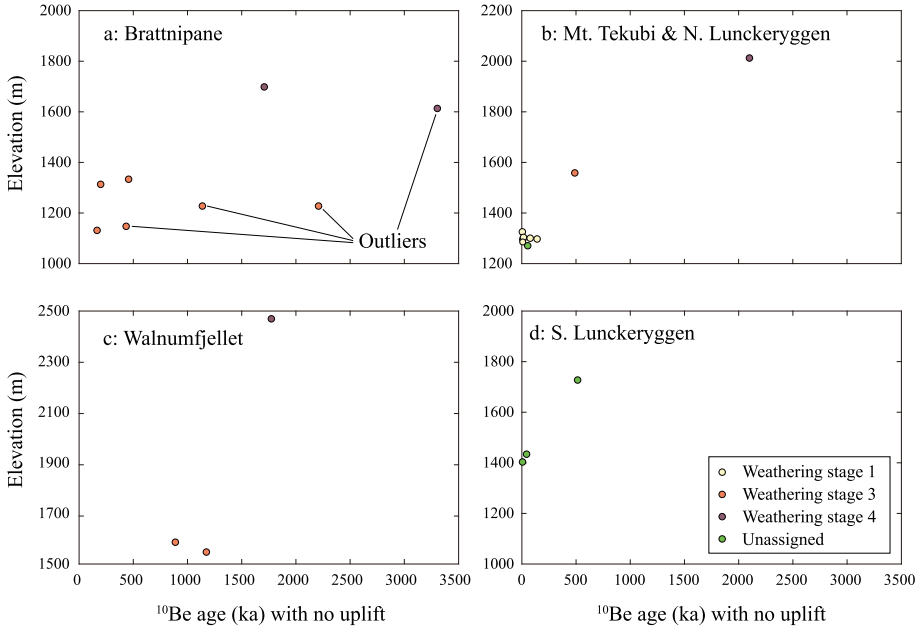

Fig. 7. ^{10}Be exposure ages versus their elevations. (a) Brattnipane, (b) Flank of Mt. Tekubi and the large moraine field at Lunckeryggen, (c) Walnumfjellet, (d) SW edge of the Lunckeryggen.

Samples 09122201 and 10012401 yield exposure ages of 479 ka and 52.4 ka, respectively. Sample 09122201 is from weathering stage 3. On the other hand, we could not assign sample 10012401 to a weathering stage because no nearby glacial deposits were found.

The six samples from weathering stage 1 at the large moraine field at Lunckeryggen yield exposure ages ranging from 3.34 ka to 138 ka (Fig. 4a). Three Last Deglaciation–Holocene dates from the right-side portion of the moraine field are consistent with the distance from the modern ice margin (Fig. 8). On the other hand, the younger age of sample 10010501 is inconsistent with a general trend of decreasing exposure ages with decreasing distance from the modern ice margin. Because this sample is from a flank of the moraine ridge and directly on the ice-core (S. Fig. 1c), this age could appear younger due to overturning. Thus, sample 10010501 is excluded from further discussion.

Except for sample 10010501, the exposure ages of samples from the flank of Mt. Tekubi and the large moraine field at Lunckeryggen are consistently trending with elevation, suggesting that the ice sheet thinning history is well recorded in these data.

4.2.3. Walnumfjellet

The three samples from Walnumfjellet fall in the age range 870–1740 ka and are found at elevations of 1567–2489 masl (Fig. 7c). Sample 10011202 is located on top of the abraded surfaces at the 2489 masl peak of the Walnumfjellet, the highest elevation places studied. The glacial striations on these abraded surfaces (Fig. 3d) show that the present-day surface was glacially polished and not eroded since the last deglaciation. The exposure age estimate from ^{10}Be for the site is 1740 ka. Samples 09122901 and 10010201 are both from weathering stage 3 and yield exposure ages of 870 ka and 1150 ka, respectively. These three results are consistent with the general trend of decreasing exposure ages with decreasing elevation.

4.2.4. SW edge of Lunckeryggen

The three samples from a large rock outcrop at the SW edge of Lunckeryggen (100111401; 10011402; 10011301) have minimum exposure ages between 4.80 ka and 504 ka (Fig. 7d). Because no glacial deposits are observed at these sites, we could not assign them to a weathering stage. The oldest sample (504 ka) is close to the highest part of the region, whereas the younger two samples (4.80 ka and 42.0 ka) are located 23 m and 54 m above the present ice surface, respectively (Fig. 3h). These two younger exposure ages are similar to those from the large moraine field at Lunckeryggen. They are consistent with the general trend of decreasing exposure ages with decreasing elevation.

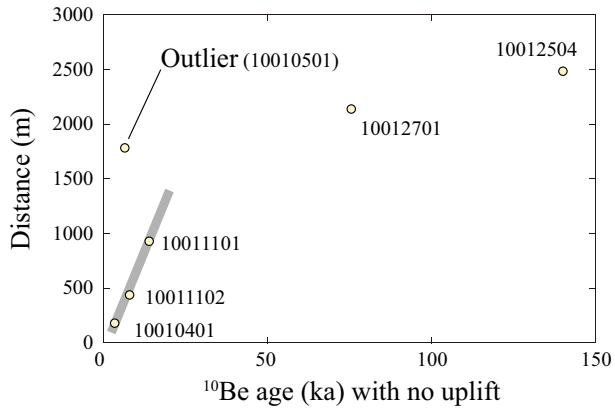

Fig. 8. ^{10}Be exposure ages versus their distance from the modern ice margin at the large moraine field at Lunckeryggen. The distance is calculated based on the longitudinal direction from the ice margin along the Jennings glacier. Sample 10010501 is considered an outlier. A trendline for the younger three samples has been drawn to guide the eye.

4.2.5. Elevation history of the ice sheet at the Sør Rondane Mountains

With the surface exposure ages that have not been rejected, we can estimate the elevation history of the ice sheet at the Sør Rondane Mountains. Fig. 9 shows ice sheet profiles of the Jennings and Byrd glaciers on a north-south geographic transect through Brattnipane to Walnumfjellet. Triangles on this transect correspond to elevations of sampled surfaces that became exposed during stages 3 and 4. From the elevation-age information, we construct former surface profiles of the ice sheet at each weathering stage. In addition, the summit of Mt Takubi lacks any evidence of ice cover in the past, indicating the height of the summit provides the upper limit of the EAIS thickness estimation (Fig. 9). These observations lead us to an interpretation in terms of a generally continuous history of ice-sheet lowering at the Sør Rondane Mountains (Fig. 10a). Elevation changes of ice sheet between the stage 4 and present are calculated from the elevations of the uppermost sample at Brattnipane and the Byrd glacier. Because the Jennings glacier flows through a relatively narrow passage between the Walnumfjellet and the SW edge of Lunckeryggen (Fig. 2), there is a small chance of overestimating ice sheet elevation at the 2489 masl peak (10011202) on Walnumfjellet.

The effect of local characteristics of the ice flow on stage 3 is probably larger than that on stage 4, because the geomorphological setting of this area becomes more complex due to lowering of the ice sheet. Although we use the Jennings glacier as a reference, estimating the elevation changes for stage 3 samples is relatively imprecise. For example, site 09121102 gives a minus value for the elevation change. We tentatively explain this by the ice flow between the Hitosashiyubi and Nakayubi Ridges having been cut by the earliest stage of lowering of ice sheet since the stage 4, cutting off supply into the valley. On the other hand, several weathering stage 3 erratics have older ages. Their geomorphological evidence suggest that they are recycled clasts, which gives some support for ice sheet level fluctuations during that stage.

5. Corrections for glacial isostatic adjustment

Crustal uplift of the central part of the Sør Rondane Mountains due to glacial rebound influences our reconstruction of its deglaciation history in two ways. Clearly, increases in elevation must be accounted for when calculating flow and thickness of glacial ice. More subtle is the effect of changing elevation with time on the production rate of ^{10}Be in all sampled rocks. Unfortunately, the lack of prior knowledge of uplift makes it impossible to directly incorporate it in the calibration between ^{10}Be concentration in quartz and exposure age. This forces us to take an iterative approach where we first calibrate the ^{10}Be results using present-day elevations, use the uncorrected ages to construct ice-sheet elevation history, and then use that as input for GIA modeling. As GIA modeling output, the region's uplift history is then used to modify the ^{10}Be production rate calibration function by introducing time-dependency to the parameter sample elevation. With the refined calibration, uplift-corrected exposure ages are derived and a new ice-sheet elevation history is constructed. To confirm the convergence to a stable set of ages and uplift history based on this calculation, we repeat this sequence of calculations once more (Table 2, Fig. 5 and S. Fig. 2). The numeric results show that the second iteration does not change the exposure ages by any significant amount. Hence, this iterative procedure, to achieve self-

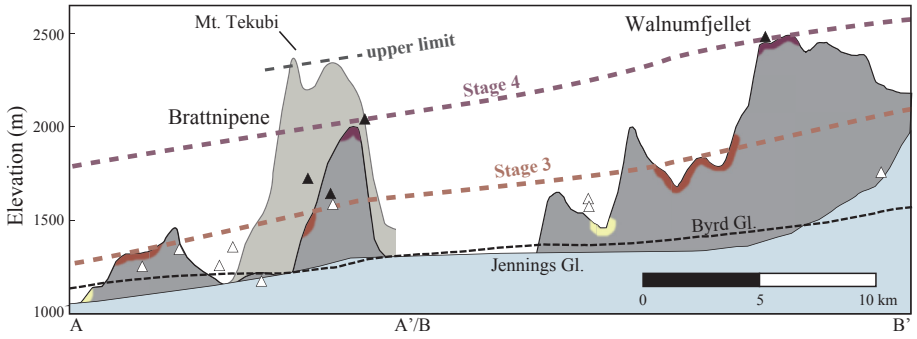

Fig. 9. Present-day ice sheet profile of the Jennings and Byrd Glaciers along geomorphological transects at the Brattnipane (A–A′) and Walnumfjellet (B–B′) drawn in Fig. 2a. Samples corresponding to weathering stages 3 and 4 are marked by white and black triangles, respectively. We use the upper limit of sample elevations belonging to each weathering stage as a marker of the former ice sheet surface. Colors are shown on the mountain profiles to highlight the different weathering stages. Mt. Tekubi is shown to represent the upper limit of former ice sheet elevation.

consistency between altitude-dependent in situ ^{10}Be production and isostatic rebound, is strongly convergent.

Because we suspect that local geomorphology and ice flow at Walnumfjellet has been responsible for a significant drop of ice sheet elevation there, this site has been excluded from the input data. The dependencies of the GIA modeling output on disk radius and mantle viscosity models for the first and second iterations are shown in Fig. 5d–f and S. Fig. 2d–f. Regardless of which viscosity model is selected, variability in total uplift is smallest for the 3° disk model (Fig. 5e). On the other hand, the 4° disk model shows larger variability of uplift values with almost the same average (Fig. 5f). This variability is most likely caused by differences in the lower mantle viscosity structure. The addition of more model dependence to the derivation of ^{10}Be exposure ages can thus, in this case, be minimized by adopting the 3° disk model.

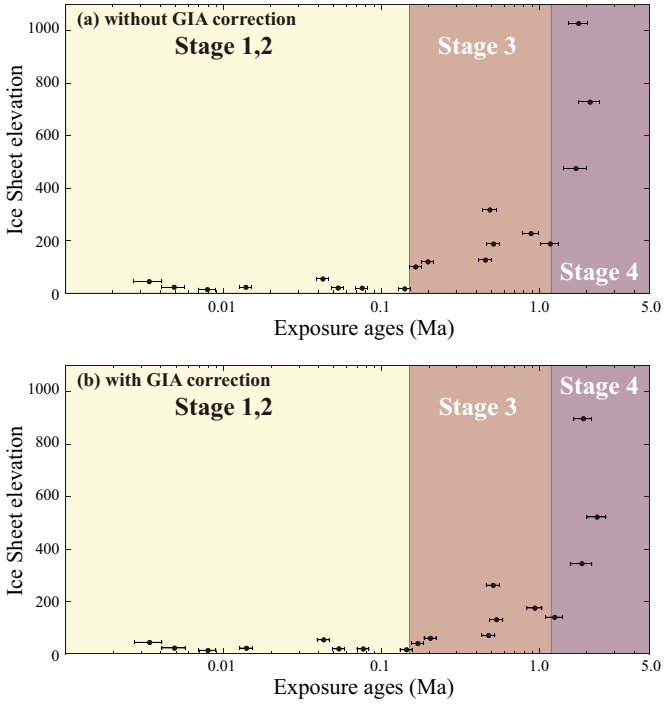

Fig. 10. Ice sheet elevation for the Sør Rondane Mountains versus ^{10}Be surface exposure ages (logarithmic scale): without (a) and with (b) uplift corrections for Glacial Isostatic Adjustment (GIA). Ice sheet elevation is constructed from the difference between sample elevations and the geomorphological transect of the Byrd glacier (Fig. 9).

Recent analysis of relative sea-level change and space geodetic observations in the Antarctic region based on GIA modeling suggests that the best-fitting Earth model for the East Antarctic sites has a lithospheric thickness of 71 km, an upper mantle viscosity of 1×10^{21} Pa s, and a lower mantle viscosity of 2×10^{21} Pa s (Whitehouse et al., 2012). In particular, GIA predictions in East Antarctica are strongly dependent on the upper mantle viscosity, but there is almost no dependence upon lower mantle viscosity. Using these mantle viscosities, we arrive at ca 206 m of isostatic rebound for the Sør Rondane Mountains since the early Pleistocene. The resulting mean uplift movements are: 158 m during 2300–1200 ka, –11 m during 1200–150 ka, and 60 m during the last 150 ka.

Subsequently, we estimate that the total amount of uplift corresponds to no more than a 10% reduction in the average ^{10}Be production rate of the longest exposed samples. Obviously, the more recent the onset of exposure the smaller this correction will be. This estimate of the size of the correction validates our approach to complete the iterative correction cycle only once. We note that a certain percentage reduction in production rate will, if all other parameters are kept constant, result in an exposure age increase by at least that same percentage. Samples for which the ^{10}Be concentration is closer to secular equilibrium of a radioactive isotope (production rate is equal to rate of decay), the age increase will be larger. We also note that, given a measure ^{10}Be concentration, increasing the sample's surface erosion rate has qualitatively a similar effect on its derived exposure age as introducing uplift.

Values for the ^{10}Be exposure ages, with and without uplift correction, are given in Table 2 and plotted against ice sheet elevation in Fig. 10. For samples used for the discussion, the uplift correction amounts up to 11% (for the oldest sample) increase in exposure ages. We infer from the corrected ages belonging to that stage that these glacial landforms emerged from beneath the EAIS during the Quaternary. Although the actual glacial history will be much more complex than we are able to reconstruct, the ^{10}Be exposure ages are evidence of ice sheet surface lowering by at least 300 m during weathering stage 3 and by no more than 50 m during weathering stages 1 and 2.

6. Discussion

6.1. Deglaciation phases

Our area of study is one of few locations available for measuring past variability in ice thickness of the interior of the EAIS. The rock weathering and ^{10}Be surface exposure data discussed in Section 4 provide the basis to identify three distinct phases of deglaciation

for the central part of the Sør Rondane Mountains in Dronning Maud Land (Fig. 11). We here discuss our findings for each phase separately.

6.1.1. Deglaciation into Pleistocene

The flat-topped ridges, the 2489 masl peak (10011202) on Walnumfjellet and the west flank (2031 masl; 09121401) of Mt. Tekubi, Brattnipane, were glacially eroded and then exposed to hyper–arid polar conditions. The summit of Mt. Tekubi, on the other hand, lacks any sign of ice sheet cover. We interpret these observations as evidence of the highest glaciation since the EAIS started growth in this region. Based on the GIA modeling, the point in time when the EAIS in this region was at least 520 m higher than at present (maximum thickness of the ice sheet is estimated have been 830 m) was during Early Pleistocene and probably Pliocene. The glacial deposits of weathering stage 4 are evidence for subsequent deglaciation. Based on the orientation of striations at the mountain top of Walnumfjellet and at the west flank of Mt. Tekubi, the EAIS was flowing in a North − 30°E direction. This is consistent with an expected flow direction of the EAIS if we assume that they overrode the Sør Rondane Mountains.

6.1.2. Middle Pleistocene fluctuation

During this phase, ice flow was more local than the Early Pleistocene, flowing the U-shaped valleys at Walnumfjellet and Brattnipane, and leaving behind the glacial deposits of weathering stage 3. Exposure ages of this stage vary from ca 1200 to 170 ka. We suspect that the erratics with older ages are clasts that have been recycled through ice sheet level fluctuations. This view is consistent with conclusions, based on joint ^{10}Be and ^{26}Al analyses in previous studies (Nishiizumi et al., 1991; Moriwaki et al., 1992; Matsuoka et al., 2006), that reburial by ice cover has taken place at the Sør Rondane Mountains.

6.1.3. Late Pleistocene–Holocene deglaciation

A key finding is that none of the exposure ages younger than the LGM occur on the glacial deposits of weathering stage 3. We would expect to find a proportion of young ages at higher elevations if the glacier had thickened during the LGM, as has been observed elsewhere in Antarctica (Ackert et al., 1999; Stone et al., 2003; Bentley et al., 2006; Mackintosh et al., 2007). Thus, it is evident that thickening of the ice sheet during the LGM was only up to ca 50 m above the present level. This explanation is also consistent with the more weathered appearance of stage 3 glacial deposits.

The five erratic samples from the Lunckeryggen moraine field vary in exposure age from 144 ka to 3.39 ka (Fig. 4a), with younger ages found toward the inside of that field (Fig. 8). This indicates that the ice sheet margin was a few kilometers more advanced than at present and that, after deposition, the erratics remained in a stable orientation. Because the moraine field is distributed within ±30 m elevation from the present ice surface level (Figs. 2b, 3e and f), significant changes of the ice sheet elevation in this phase can be ruled out. However, as can be seen in Fig. 8, samples 10011101 and 10012701 do not follow the age–distance trend of the three younger samples. This suggests that the ice stream was thinned or stable after deposition of sample 10012701 and then expanded during the LGM. Although no exposure ages are available, the glacial deposits distributed between Oyayubi and Hitosashiyubi Ridges at Brattnipane are also associated with this phase, based on their degree of weathering. The two younger samples from the southwest edge of the Lunckeryggen and the one sample from the deep valley between the Nakayubi and Kusuriyubi Ridges provide the evidence for ca 50 masl of ice expansion during the LGM.

As mentioned above, young exposure age samples are only found in the large moraine field along the modern-day ice margins. This clearly indicates that, in the Sør Rondane Mountains, ice sheet thinning was completed by ca 140 ka. Furthermore, the limited change in ice sheet elevation during and since marine isotope stage 5e (MIS 5e) up until the LGM suggests glacial/interglacial stability in ice thickness of the EAIS's interior.

6.2. Link to climate evolution into the Pleistocene

6.2.1. EAIS thinning and reorganization of Southern Ocean circulation into Pleistocene

Our finding of significant thinning of the EAIS in Dronning Maud Land sector is compatible with results of other workers who have presented evidence of former high ice stands in other regions of the EAIS: Lambert Glacier-Amery Ice Shelf graben (Fink et al., 2006; Huang et al., 2008; Kong et al., 2010; Lilly et al., 2010; Liu et al., 2010), Queen (Dronning) Maud Land (Altmaier et al., 2010), the Coats Land sector (Fogwill et al., 2004), and Victoria Land sector of the Transantarctic Mountains (Strasky et al., 2009; Di Nicola et al., 2009, 2012). Although several studies suggest maximum Antarctic ice sheet during middle Miocene (Fogwill et al., 2004; Di Nicola et al., 2009, 2012), most of these studies report a significant thinning of the ice sheet since the Plio-Pleistocene. Liu et al. (2010) suggest that the ice surface in the Grove Mountains region rose to more than 200 m above the present-day elevation during the Middle Pliocene Climatic Warm Event (3.29–2.97 Ma). Yet, during the early Pliocene, globally averaged surface temperatures were ~3 °C higher than at present (Haywood et al., 2013). An explanation has been given for this apparent contradiction: in a warmer global climate, poleward warmer transport from the Southern Ocean is increased, which contributes to ice sheet growth (Altmaier et al., 2010; Kong et al., 2010). The results of our study are consistent with the argument that cooling and expansion of sea ice on the Southern Ocean restricted poleward movement of moisture (e.g., McKay et al., 2012), causing a reduction in the height of the EAIS in Dronning Maud Land.

The Southern Ocean has a profound influence on the world's oceans and climate (e.g., Carter et al., 2008). In several studies it has been proposed that the EAIS responds to global climate events, such as the late-Pliocene global cooling, mid-Pleistocene transition, and Mid-Brunhes event, through the meridional migration of zonal westerly winds and Southern Ocean fronts (e.g., Bard and Rickaby, 2009; Kemp et al., 2010; McKay et al., 2012). More recently, McKay et al. (2012) proposed that ice sheet expansion in West Antarctica and cooling in the Southern Ocean led to an increased seasonal persistence of sea ice between 3.3 and 2.6 Ma, which is thought to have affected the northward expansion of westerly winds and the northward migration of ocean fronts in the Southern Ocean. They suggest that this situation contributed to a restriction of flow of the Agulhas Current to the south Atlantic that controls the heat and salt from the Indo-Pacific Ocean to the Atlantic Ocean (e.g. Bard and Rickaby, 2009), ultimately leading to a slowdown of the inter-hemispheric Atlantic Meridional Overturning Circulation (AMOC) beginning after 2.6 Ma. It would also have further intensified the cooling into the Pleistocene. The northward migration of ocean fronts of the Southern Ocean, simply expressed by the Antarctic Circumpolar Current (ACC), is thought to cause a north-east expansion of the Weddel Gyre and expansion of seasonal sea ice coverage (Fig. 12). This particular connection between seasonal sea ice coverage and global climate is consistent with reconstructions made by Allen et al. (2011) for the Last Glacial period. This phenomenon probably has restricted or reduced the southward moisture transport from adjacent area of the Southern Ocean, and thus decreased the thickness of the EAIS into the Pleistocene.

This view of a high ice sheet in East Antarctic does not contradict reconstructions of global mean sea level much higher than today

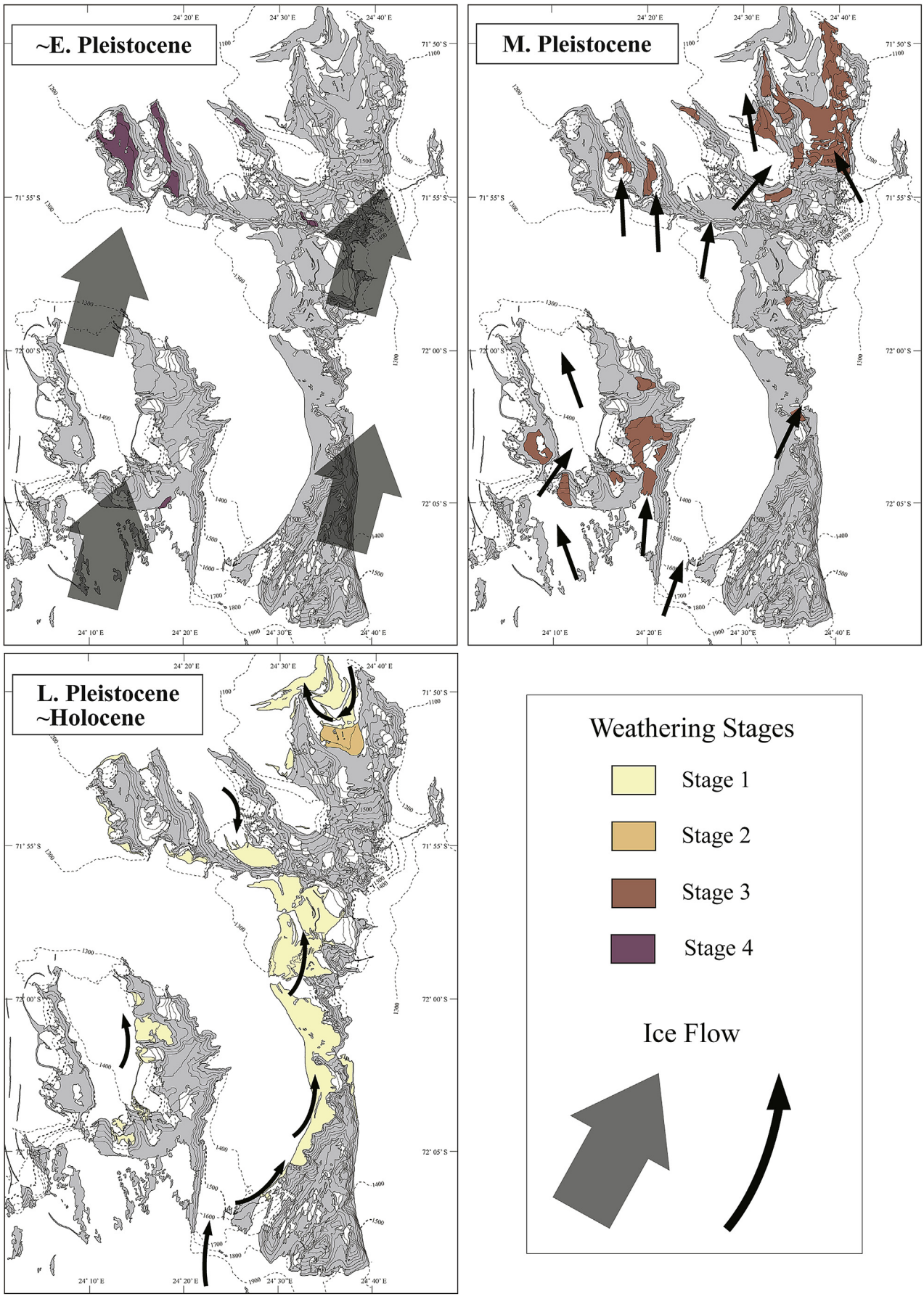

Fig. 11. Deglaciation history of the Sør Rondane Mountains. Three distinct deglaciation phases are identified. During the Pliocene, the EAIS was overriding the mountain, as shown with the large black arrows. Their direction is N15°E: the mean direction of glacial striations on the top of Walnumfjellet and at the west flank of Mt. Tekubi (North − 30°E). In the diagrams for the other two deglaciation phases, small black arrows portray more local ice flow along the U-shaped valley at Walnumfjellet and Brattnipane (early–mid. Pleistocene) and along the moraine fields (late Pleistocene–Holocene).

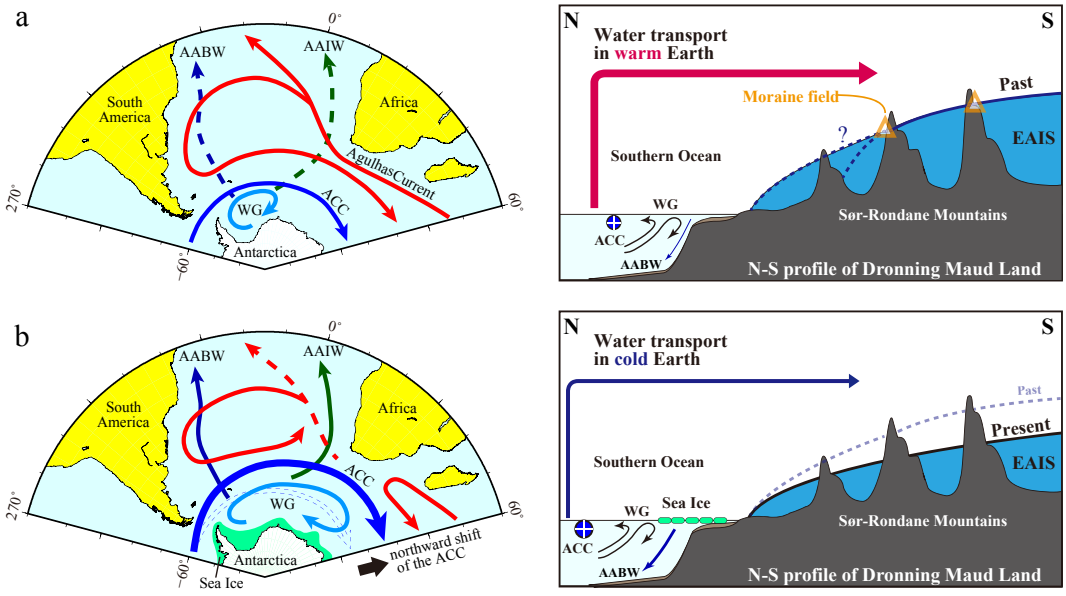

Fig. 12. Schematic representation of the reorganization of the Southern Ocean circulation since late Pliocene. ACC = Antarctic Circumpolar Current, WG = Weddell Gyre, AAIW = Antarctic Intermediate Water, and AABW = Antarctic Bottom Water.

during the Pliocene. Miller et al. (2012) reports ~22 m higher sea-level than present for the Pliocene interval 2.7–3.2 Ma and suggests ~10 m sea-level equivalent loss from the EAIS. Loss of ice from marine-based costal margins of the EAIS accounts for 20% reduction in EAIS volume, even though increased precipitation in the interior was causing the EAIS to thicken (e.g., Cook et al., 2013). Climatic models also show a stability of most part of the EAIS, with volume changes along Wilkes Margin and in inlets such as Prydz Bay contributing to high eustatic sea-level during Pliocene (DeConto and Pollard, 2003; Pollard and DeConto, 2009). Based on the lines of evidence of the high ice stand from Dronning Maud Land, Transantarctic Mountains, and Lambert Glacier-Amery Ice Shelf graben, we especially emphasize that Wilkes Basin and Aurora Basin are a possible source of the ice mass loss. This view is clearly supported by the recent Bedmap2 project, which shows that the large area of Wilkes Land sector of EAIS is grounded below present sea-level (Fretwell et al., 2013).

6.2.2. Response to post-LGM warming

The retreat of the EAIS is attributed to both sea-level rise and warming of the ocean at the margin of the ice sheet (e.g., Mackintosh et al., 2011). Mackintosh et al. (2013) shows that the EAIS ice sheet advanced to the middle or mid-outer continental shelf during the LGM, with the exception of the Lützow Holm Bay, Dronning Maud Land, where it is possible that there was no advance (Miura et al., 1998). Several hundred meters of thicker ice sheet before the last deglaciation is also suggested by exposure ages from Mac. Robertson Land (Mackintosh et al., 2007), Prince Charles Mountains (White et al., 2011), and Lützow Holm Bay (Yamane et al., 2011).

In contrast, our exposure ages indicate that since LGM the ice surface reached an elevation of no more than 50 m above its current elevation. Such a muted response to the LGM is also reported for the interior of the EAIS at Grove Mountains in Lambert Glacier-Amery Ice Shelf graben (Lilly et al., 2010) and Ferrar Glacier in southern Victoria Land (Staiger et al., 2006). Based on climate-driven thermomechanical ice sheet models and glacio-hydro-isostatic ice sheet models, a change in ice sheet thickness from the LGM relative to the present is predicted (e.g., Nakada et al., 2000; Huybrechts, 2002; Ivins and James, 2005; Whitehouse et al., 2012). Ivins and James (2005) indicate that spatially homogeneous climatic conditions prevailed in the interior of East Antarctica throughout glacial times. Ice sheet thinning of interior of the EAIS is almost negligible, which is consistent with our results. Similarly, simulation of Antarctic deglaciation with a continental ice-sheet model shows that ice sheet loss occurs at the margin of both the EAIS and the WAIS, mostly at the present-day continental shelf (Mackintosh et al., 2011). This model even indicates a small postglacial thickening of the EAIS interior due to increased accumulation. In addition, as mentioned before, Allen et al. (2011) reported expansions of winter and summer sea ice coverage at the Atlantic sector of the Southern Ocean during the LGM and pre-LGM (30–22 ka), respectively. This phenomenon is also consistent with the muted response of the EAIS interior during the LGM due to the restricted poleward movement of moisture from the Southern Ocean.

A large, rapid meltwater discharge event, MWP-1A, was initially identified in the coral-based sea-level record from Barbados (Fairbanks, 1989) where a sea-level rise of 20 m at ca 14 ka was inferred. Recently, Deschamps et al. (2012) provided the detailed timing (14.30–14.65 ka) and magnitude (~14 m) of the MWP-1A, based on corals drilled offshore from Tahiti. Two conflicting scenarios have been proposed to link the timing and source(s) of MWP-1A: Northern Hemisphere ice sheets (Fairbanks, 1989; Peltier, 2005), and Antarctic ice sheets (Clark et al., 2002; Bassett et al., 2005, 2007).

The Northern Hemisphere ice sheets, especially the Laurentide Ice Sheet, have commonly been considered as the sole source for MWP-1A, because they account for more than 80% of total sea-level rise during the last deglaciation (Fairbanks, 1989). On the other hand, two studies suggest that, based on GIA modeling of the geographic distribution of sea-level rise (sea-level fingerprints), Antarctic ice sheet melting is a major contributor to MWP-1A (Clark et al., 2002; Bassett et al., 2005). By further constraining their GIA modeling calculations with relative sea-level records along the Antarctic coast, Bassett et al. (2007) cannot rule out the possibility that the Antarctic ice sheets have significantly contributed to MWP-1A. However, the relative sea-level records used in that study are

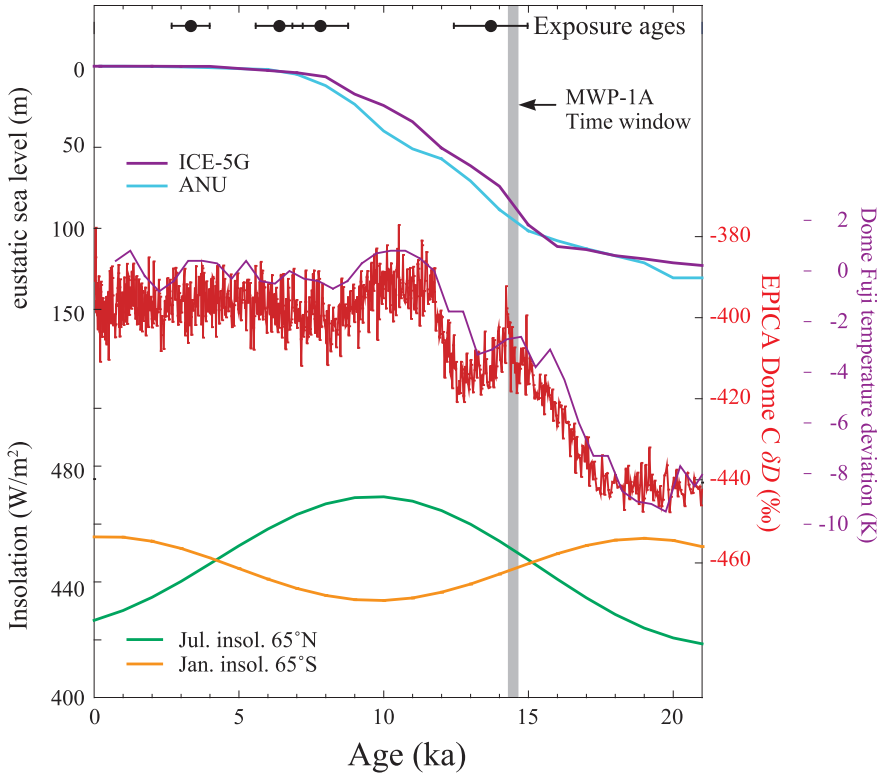

Fig. 13. Post-LGM ^{10}Be surface exposure ages compared with paleoclimatic proxies. The exposure age data are taken from Table 2. Proxy records shown are eustatic sea-level rise determined by the GIA models (ICE-5G, Peltier, 2004; ANU, Lambeck and Chappell, 2001), EPICA Dome C deuterium-isotope (Augustin et al., 2004), Dome Fuji temperature deviation (ΔT_{site}) (Kawamura et al., 2007), and 65°N and 65°S summer solstice insolations. The gray-shaded time window shows the tight chronological constraints derived for MWP-1A from the Tahiti record (Deschamps et al., 2012).

only available after 12 ka, which makes it difficult to present direct evidence of retreat of the Antarctic ice sheets associated with MWP-1A (14.30–14.65 ka). Whitehouse et al. (2012) propose a new deglaciation model for Antarctica ice sheet derived from numerical modeling (GIA and ice-sheet model) and tightly constrained by geological data. In that model, the total contribution of Antarctic ice sheet melting after the LGM is less than 9 m equivalent sea-level rise. They conclude that the excess volume of Antarctic ice sheet available around 14.5 ka was too small to be the dominant source for MWP-1A (Whitehouse et al., 2012).

Our data support limited thinning of this sector of EAIS since the LGM, implying a minimal contribution to MWP-1A. Fig. 13 compares deglaciation at Sør Rondane Mountains with eustatic sea-level change curves (Lambeck and Chappell, 2001; Peltier, 2004) and with the air temperature reconstruction from the EPICA Dome C ice core (Augustin et al., 2004). These eustatic sea-level curves are deduced by GIA predictions and far-field sea-level observations (e.g., Barbados, Tahiti and Australia, etc.). Our data suggest that retreat of this region of the EAIS post-dates MWP-1A and that during this period the EAIS lost too little ice to be noticeable. This indicates that this sector of the EAIS has not made a significant contribution to global sea-level rise during MWP-1A. This view is in line with studies of the ice sheet margins of East Antarctica (e.g., Mackintosh et al., 2011).

7. Conclusions

In this study, we reconstruct a detailed glacial history in the central part of the Sør Rondane Mountains in Dronning Maud Land, East Antarctica, based on geomorphological survey, cosmogenic exposure dating, and glacial isostatic adjustment (GIA) modeling. Based on the weathering index dada (Moriwaki index), these glacial till deposits have been divided into four stages. ^{10}Be surface exposure ages from 23 erratic boulders and bedrocks at 1132–2470 masl vary from 3.39 to 2319 ka and, out of these 18, were used for discussion and interpretation. They generally increase as a function of increasing elevation above the current ice sheet surface, indicating a long-term decrease in ice thickness of this sector of the EAIS. To obtain a more precise estimate of thinning of the EAIS, the crustal uplift of the central part of the Sør Rondane Mountains due to glacial rebound is estimated with GIA modeling. These data provide the basis for the identification of three distinct phases of the deglaciation history of the central part of the Sør Rondane Mountains in Dronning Maud Land:

1. The ice sheet thickness in the Sør Rondane Mountains area, East Antarctica, decreased at least 500 m since the Early Pleistocene.
2. This thinning was caused by a reduction in moisture transport from the Southern Ocean to the interior of the EAIS, probably due to a reorganization of the Southern Ocean circulation.
3. Our data reveal that thinning of Dronning Maud Land sector of EAIS since the LGM was relatively small and probably started after ca 14 ka. This indicates that this sector of the EAIS is unlikely to have been a major contributor to postglacial sea-level rise and Meltwater pulse 1A.

Acknowledgments

We are grateful for the constructive comments of Jon Harbor and a second anonymous reviewer. The study was supported by the Japanese Antarctic Research Expedition and partially funded by JSPS Kakenhi (21253001, 21674003, 20300294, and 00344614), the

Sumitomo Foundation (093491), a Sasakawa Scientific Research Grant (JSS-21-334), the Center for the Promotion of Integrated Sciences (CPIS) of Sokendai, and NIPR through Advanced Project (KP-1). The production of this paper was supported by an NIPR publication subsidy. We thank Alan Hubert, Gigi, and all members at PE station (Belgium). We are also grateful for the help given by Mark Quigley at the University of Canterbury, New Zealand.

Appendix A. Supplementary material

Supplementary data related to this article can be found at http://dx.doi.org/10.1016/j.quascirev.2014.05.007.

References

Ackert Jr., R.P., Barclay, D.J., Borns Jr., H.W., Calkin, P.E., Kurz, M.D., Fastook, J.L., Steig, E.J., 1999. Measurements of past ice sheet elevations in interior West Antarctica. Science 286, 276–280.

Allen, C.S., Pike, J., Pudsey, C.J., 2011. Last glacial–interglacial sea-ice cover in the SW Atlantic and its potential role in global deglaciation. Quat. Sci. Rev. 30, 2446–2458.

Altmaier, M., Herpers, U., Delisle, G., Merchel, S., Ott, U., 2010. Glaciation history of Queen Maud Land (Antarctica) reconstructed from in-situ produced cosmogenic ^{10}Be, ^{26}Al and ^{21}Ne. Polar Sci. 4, 42–61.

Aniya, M., 1989. Landforms of the Balchenfjella Area, the Sør Rondane, East Antarctica. Proc. NIPR Symp. Antarct. Geosci. 3, 353–375.

Argus, D.F., Peltier, W.R., 2010. Constraining models of postglacial rebound using space geodesy: a detailed assessment of model ICE-5G (VM2) and its relatives. Geophys. J. Int. 181, 697–723.

Augustin, L., Barbante, C., Barnes, P.R.F., Barnola, J.M., Bigler, M., Castellano, E., Cattani, O., Chappellaz, J., DahlJensen, D., Delmonte, B., Dreyfus, G., Durand, G., Falourd, S., Fischer, H., Fluckiger, J., Hansson, M.E., Huybrechts, P., Jugie, R., Johnsen, S.J., Jouzel, J., Kaufmann, P., Kipfstuhl, J., Lambert, F., Lipenkov, V.Y., Littot, G.V.C., Longinelli, A., Lorrain, R., Maggi, V., Masson-Delmotte, V., Miller, H., Mulvaney, R., Oerlemans, J., Oerter, H., Orombelli, G., Parrenin, F., Peel, D.A., Petit, J.R., Raynaud, D., Ritz, C., Ruth, U., Schwander, J., Siegenthaler, U., Souchez, R., Stauffer, B., Steffensen, J.P., Stenni, B., Stocker, T.F., Tabacco, I.E., Udisti, R., van de Wal, R.S.W., van den Broeke, M., Weiss, J., Wilhelms, F., Winther, J.G., Wolff, E.W., Zucchelli, M., 2004. Eight glacial cycles from an Antarctic ice core. Nature 429, 623–628.

Balco, G., 2011. Contributions and unrealized potential contributions of cosmogenic-nuclide exposure dating to glacier chronology, 1990–2010. Quat. Sci. Rev. 30, 3–27.

Balco, G., Stone, J.O., Lifton, N.A., Dunai, T.J., 2008. A complete and easily accessible means of calculating surface exposure ages or erosion rates from ^{10}Be and ^{26}Al measurements. Quat. Geochronol. 3, 174–195.

Bard, E., Rickaby, R.E.M., 2009. Migration of the subtropical front as a modulator of glacial climate. Nature 460, 380–383.

Bassett, S.E., Milne, G.A., Bentley, M.J., Huybrechts, P., 2007. Modelling Antarctic sea-level data to explore the possibility of a dominant Antarctic contribution to meltwater pulse IA. Quat. Sci. Rev. 26, 2113–2127.

Bassett, S.E., Milne, G.A., Mitrovica, J.X., Clark, P.U., 2005. Climate change: ice sheet and solid earth influences on far-field sea-level histories. Science 309, 925–928.

Bentley, M.J., Fogwill, C.J., Kubik, P.W., Sugden, D.E., 2006. Geomorphological evidence and cosmogenic ^{10}Be/^{26}Al exposure ages for the last glacial maximum and deglaciation of the Antarctic Peninsula Ice Sheet. Bull. Geol. Soc. Am. 118, 1149–1159.

Bindoff, N.L., Willebrand, J., Artale, V., Cazenave, A., Gregory, J., Gulev, S., Hanawa, K., Le Quéré, C., Levitus, S., Nojiri, Y., Shum, C.K., Talley, L.D., Unnikrishnan, A., 2007. Observations: oceanic climate change and sea level. In: Solomon, S., Qin, D., Manning, M., Chen, Z., Marquis, M., Averyt, K.B., Tignor, M., Miller, H.L. (Eds.), Climate Change 2007: The Physical Science Basis. Contribution of Working Group I to the Fourth Assessment Report of the Intergovernmental Panel on Climate Change. Cambridge University Press, Cambridge, United Kingdom and New York, NY, USA (Chapter 5).

Brook, E.J., Brown, E.T., Kurz, M.D., Ackert Jr., R.P., Raisbeck, G.M., Yiou, F., 1995. Constraints on age, erosion, and uplift of Neogene glacial deposits in the Transantarctic Mountains determined from in situ cosmogenic ^{10}Be and ^{26}Al. Geology 23, 1063–1066.

Carter, L., McCave, I.N., Williams, M.J.M., 2008. Circulation and water masses of the Southern Ocean: a review. In: Florindo, F., Siegert, M. (Eds.), Developments in Earth & Environmental Sciences, vol. 8. Elsevier Science, pp. 85–114.

Child, D., Elliott, G., Mifsud, C., Smith, A.M., Fink, D., 2000. Sample processing for earth science studies at ANTARES. Nucl. Instrum. Methods Phys. Res. B: Beam Interact. Mater. Atoms 172, 856–860. http://dx.doi.org/10.1016/S0168-583X(00)00198-1.

Clark, P.U., Mitrovica, J.X., Milne, G.A., Tamisiea, M.E., 2002. Sea-level fingerprinting as a direct test for the source of global meltwater pulse IA. Science 295, 2438–2441.

Cook, C.P., van de Flierdt, T., Williams, T., Hemming, S.R., Iwai, M., Kobayashi, M., Jimenez-Espejo, F.J., Escutia, C., Gonzalez, J.J., Khim, B.-K., McKay, R.M., Passchier, S., Bohaty, S.M., Riesselman, C.R., Tauxe, L., Sugisaki, S., Galindo, A.L., Patterson, M.O., Sangiorgi, F., Pierce, E.L., Brinkhuis, H., Klaus, A., Fehr, A., Bendle, J.A.P., Bijl, P.K., Carr, S.A., Dunbar, R.B., Flores, J.A., Hayden, T.G., Katsuki, K., Kong, G.S., Nakai, M., Olney, M.P., Pekar, S.F., Pross, J., Rohl, U., Sakai, T., Shrivastava, P.K., Stickley, C.E., Tuo, S., Welsh, K., Yamane, M., 2013. Dynamic behaviour of the East Antarctic ice sheet during Pliocene warmth. Nat. Geosci. 6, 765–769.

DeConto, R.M., Pollard, D., 2003. Rapid Cenozoic glaciation of Antarctica induced by declining atmospheric CO_2. Nature 421, 245–249.

Deschamps, P., Durand, N., Bard, E., Hamelin, B., Camoin, G., Thomas, A.L., Henderson, G.M., Okuno, J., Yokoyama, Y., 2012. Ice-sheet collapse and sea-level rise at the Bølling warming 14,600 years ago. Nature 483, 559–564.

Di Nicola, L., Baroni, C., Strasky, S., Salvatore, M.C., Schlüchter, C., Açkar, N., Kubik, P.W., Wieler, R., 2012. Multiple cosmogenic nuclides document the stability of the East Antarctic Ice Sheet in northern Victoria Land since the Late Miocene (5–7 Ma). Quat. Sci. Rev. 57, 85–94.

Di Nicola, L., Strasky, S., Schlüchter, C., Salvatore, M.C., Açkar, N., Kubik, P.W., Christl, M., Kasper, H.U., Wieler, R., Baroni, C., 2009. Multiple cosmogenic nuclides document complex Pleistocene exposure history of glacial drifts in Terra Nova Bay (northern Victoria Land, Antarctica). Quat. Res. 71, 83–92.

Dunne, J., Elmore, D., Muzikar, P., 1999. Scaling factors for the rates of production of cosmogenic nuclides for geometric shielding and attenuation at depth on sloped surfaces. Geomorphology 27, 3–11.

Dziewonski, A.M., Anderson, D.L., 1981. Preliminary reference Earth model. Phys. Earth Planet. Interiors 25, 297–356.

Fairbanks, R.G., 1989. A 17,000 year glacio-eustatic sea-level record: influence of glacial melting rates on the Younger Dryas event and deep ocean circulation. Nature 342, 637–642.

Fink, D., McKelvey, B., Hambrey, M.J., Fabel, D., Brown, R., 2006. Pleistocene deglaciation chronology of the Amery Oasis and Radok Lake, northern Prince Charles Mountains, Antarctica. Earth Planet. Sci. Lett. 243, 229–243.

Fogwill, C.J., Bentley, M.J., Sugden, D.E., Kerr, A.R., Kubik, P.W., 2004. Cosmogenic nuclides ^{10}Be and ^{26}Al imply limited Antarctic Ice Sheet thickening and low erosion in the Shackleton Range for >1 m.y. Geology 32, 265–268.

Fretwell, P., Pritchard, H.D., Vaughan, D.G., Bamber, J.L., Barrand, N.E., Bell, R., Bianchi, C., Bingham, R.G., Blankenship, D.D., Casassa, G., Catania, G., Callens, D., Conway, H., Cook, A.J., Corr, H.F.J., Damaske, D., Damm, V., Ferraccioli, F., Forsberg, R., Fujita, S., Gim, Y., Gogineni, P., Griggs, J.A., Hindmarsh, R.C.A., Holmlund, P., Holt, J.W., Jacobel, R.W., Jenkins, A., Jokat, W., Jordan, T., King, E.C., Kohler, J., Krabill, W., Riger-Kusk, M., Langley, K.A., Leitchenkov, G., Leuschen, C., Luyendyk, B.P., Matsuoka, K., Mouginot, J., Nitsche, F.O., Nogi, Y., Nost, O.A., Popov, S.V., Rignot, E., Rippin, D.M., Rivera, A., Roberts, J., Ross, N., Siegert, M.J., Smith, A.M., Steinhage, D., Studinger, M., Sun, B., Tinto, B.K., Welch, B.C., Wilson, D., Young, D.A., Xiangbin, C., Zirizzotti, A., 2013. Bedmap2: improved ice bed, surface and thickness datasets for Antarctica. Cryosphere 7, 375–393.

Gosse, J.C., Phillips, F.M., 2001. Terrestrial in situ cosmogenic nuclides: theory and application. Quat. Sci. Rev. 20, 1475–1560.

Hansen, C.D., Meiklejohn, K.I., Nel, W., Loubser, M.J., Van Der Merwe, B.J., 2013. Aspect-controlled weathering observed on a Blockfield in Dronning Maud Land, Antarctica. Geogr. Ann. Ser. A, Phys. Geogr. 95, 305–313.

Hayashi, M., Miura, K., 1989. Glacial landforms and weathering processes in the Balchenfjella region, Eastern part of the Sør Rondane Mountains, East Antarctica. Proc. NIPR Symp. Antarct. Geosci. 3, 65–80.

Haywood, A.M., Hill, D.J., Dolan, A.M., Otto-Bliesner, B.L., Bragg, F., Chan, W.L., Chandler, M.A., Contoux, C., Dowsett, H.J., Jost, A., Kamae, Y., Lohmann, G., Lunt, D.J., Abe-Ouchi, A., Pickering, S.J., Ramstein, G., Rosenbloom, N.A., Salzmann, U., Sohl, L., Stepanek, C., Ueda, H., Yan, Q., Zhang, Z., 2013. Large-scale features of Pliocene climate: results from the Pliocene model intercomparison project. Clim. Past 9, 191–209.

Hirakawa, K., Moriwaki, K., 1990. Former ice sheet based on the newly observed glacial landforms and erratics in the central Sør Rondane Mountains, East Antarctica. Proc. NIPR Symp. Antarct. Geosci. 4, 41–54.

Hirakawa, K., Matsuoka, N., Moriwaki, K., 1988. Reconstruction of maximum glacial extent in the Sør Rondane Mountains, East Antarctica. Proc. NIPR Symp. Antarct. Geosci. 2, 146–161.

Huang, F., Liu, X., Kong, P., Fink, D., Ju, Y., Fang, A., Yu, L., Li, X., Na, C., 2008. Fluctuation history of the interior East Antarctic Ice Sheet since mid-Pliocene. Antarct. Sci. 20, 197–203.

Huber, M., Brinkhuis, H., Stickley, C.E., Döös, K., Sluijs, A., Warnaar, J., Schellenberg, S.A., Williams, G.L., 2004. Eocene circulation of the Southern Ocean: was Antarctica kept warm by subtropical waters? Paleoceanography 19, 1–12.

Hughes, I., Hase, T., 2010. Measurements and Their Uncertainties: a Practical Guide to Modern Error Analysis. Oxford University Press, 160 pp.

Huybrechts, P., 2002. Sea-level changes at the LGM from ice-dynamic reconstructions of the Greenland and Antarctic ice sheets during the glacial cycles. Quat. Sci. Rev. 21, 203–231.

Ivins, E.R., James, T.S., 2005. Antarctic glacial isostatic adjustment: a new assessment. Antarct. Sci. 17, 541–553.

Ivy-Ochs, S., Schluchter, C., Kubik, P.W., Dittrich-Hannen, B., Beer, J., 1995. Minimum ^{10}Be exposure ages of early Pliocene for the Table Mountain plateau and the Sirius Group at Mount Fleming, Dry Valleys, Antarctica. Geology 23, 1007–1010.

Iwata, S., 1987. Debris-mantled rectilinear slopes in the western Sør Rondane Mountains, East Antarctica. Proc. NIPR Symp. Antarct. Geosci. 1, 178–192.
Kawamura, K., Parrenin, F., Lisiecki, L., Uemura, R., Vimeux, F., Severinghaus, J.P., Hutterli, M.A., Nakazawa, T., Aoki, S., Jouzel, J., Raymo, M.E., Matsumoto, K., Nakata, H., Motoyama, H., Fujita, F., Goto-Azuma, K., Fujii, Y., Watanabe, O., 2007. Northern Hemisphere forcing of climatic cycles in Antarctica over the past 360,000 years. Nature 448, 912–916.
Kemp, A.E.S., Grigorov, I., Pearce, R.B., Naveira Garabato, A.C., 2010. Migration of the Antarctic polar front through the mid-Pleistocene transition: evidence and climatic implications. Quat. Sci. Rev. 29, 1993–2009.
Kong, P., Huang, F., Liu, X., Fink, D., Ding, L., Lai, Q., 2010. Late Miocene ice sheet elevation in the Grove Mountains, East Antarctica, inferred from cosmogenic ^{21}Ne–^{10}Be–^{26}Al. Global Planet. Change 72, 50–54.
Lal, D., 1991. Cosmic ray labeling of erosion surfaces: in situ nuclide production rates and erosion models. Earth Planet. Sci. Lett. 104, 424–439.
Lambeck, K., Chappell, J., 2001. Sea level change through the last glacial cycle. Science 292, 679–686.
Lilly, K., Fink, D., Fabel, D., Lambeck, K., 2010. Pleistocene dynamics of the interior East Antarctic ice sheet. Geology 38, 703–706.
Liu, X., Huang, F., Kong, P., Fang, A., Li, X., Ju, Y., 2010. History of ice sheet elevation in East Antarctica: Paleoclimatic implications. Earth Planet. Sci. Lett. 90, 281–288.
Mackintosh, A., Golledge, N., Domack, E., Dunbar, R., Leventer, A., White, D., Pollard, D., Deconto, R., Fink, D., Zwartz, D., Gore, D., Lavoie, C., 2011. Retreat of the East Antarctic ice sheet during the last glacial termination. Nat. Geosci. 4, 195–202.
Mackintosh, A., White, D., Fink, D., Gore, D.B., Pickard, J., Fanning, P.C., 2007. Exposure ages from mountain dipsticks in Mac. Robertson Land, East Antarctica, indicate little change in ice-sheet thickness since the Last Glacial Maximum. Geology 35, 551–554.
Mackintosh, A.N., Verleyen, E., O'Brien, P.E., White, D.A., Jones, R.S., McKay, R., Dunbar, R., Gore, D.B., Fink, D., Post, A.L., Miura, H., Leventer, A., Goodwin, I., Hodgson, D.A., Lilly, K., Crosta, X., Golledge, N.R., Wagner, B., Berg, S., van Ommen, T., Zwartz, D., Roberts, S.J., Vyverman, W., Masse, G., 2013. Retreat history of the East Antarctic Ice Sheet since the Last Glacial Maximum. Quat. Sci. Rev. http://dx.doi.org/10.1016/j.quascirev.2013.07.024.
Masarik, J., Wieler, R., 2003. Production rates of cosmogenic nuclides in boulders. Earth Planet. Sci. Lett. 216, 201–208.
Matsuoka, N., Thomachot, C.E., Oguchi, C.T., Hatta, T., Abe, M., Matsuzaki, H., 2006. Quaternary bedrock erosion and landscape evolution in the Sor Rondane Mountains, East Antarctica: reevaluating rates and processes. Geomorphology 81, 408–420.
McKay, R., Naish, T., Carter, L., Riesselman, C., Dunbar, R., Sjunneskog, C., Winter, D., Sangiorgi, F., Warren, C., Pagani, M., Schouten, S., Willmott, V., Levy, R., DeConto, R., Powell, R.D., 2012. Antarctic and Southern Ocean influences on Late Pliocene global cooling. Proc. Natl. Acad. Sci. U. S. A. 109, 6423–6428.
Mifsud, C., Fujioka, T., Fink, D., 2013. Extraction and purification of quartz in rock using hot phosphoric acid for in situ cosmogenic exposure dating. Nucl. Instrum. Methods Phys. Res. B: Beam Interact. Mater. Atoms 294, 203–207. http://dx.doi.org/10.1016/j.nimb.2012.08.037.
Miller, K.G., Wright, J.D., Browning, J.V., Kulpecz, A., Kominz, M., Naish, T.R., Cramer, B.S., Rosenthal, Y., Peltier, W.R., Sosdian, S., 2012. High tide of the warm pliocene: implications of global sea level for Antarctic deglaciation. Geology 40, 407–410.
Miura, H., Maemoku, H., Igarashi, A., Moriwaki, K., 1998. Late Quaternary raised beach deposits and radiocarbon dates of marine fossils around Lützow-Holm Bay. In: Special Map Series of National Institute of Polar Research, vol. 6. National Institute of Polar Research, Tokyo, 46 pp.
Moriwaki, K., Hirakawa, K., Hayashi, M., Iwata, S., 1992. Late Cenozoic Glacial history in the Sør-Rondane Mountains, East Antarctica. In: Yoshida, Y., Kaminuma, K., Shiraishi, K. (Eds.), Recent Progress in Antarctic Earth Science. Terra Scientific Publishing Company, Tokyo, pp. 661–667.
Moriwaki, K., Iwata, S., Matsuoka, N., Hasegawa, H., Hirakawa, K., 1991. Weathering stage of till and glacial history of the central Sør-Rondane Mountains. Proc. NIPR Symp. Antarct. Geosci. 5, 99–111.
Moriwaki, K., Iwata, S., Matsuoka, N., Hasegawa, H., Hirakawa, K., 1994. Weathering stage as a relative age of till in the central Sør-Rondane. Proc. NIPR Symp. Antarct. Geosci. 7, 156–161.
Müller, A.M., Christl, M., Döbeli, M., Kubik, P.W., Suter, M., Synal, H.A., 2010. Boron suppression with a gas ionization chamber at very low energies ($E < 1$ MeV). Nucl. Instrum. Methods Phys. Res. B: Beam Interact. Mater. Atoms 268, 843–846. http://dx.doi.org/10.1016/j.nimb.2009.10.045.
Nakada, M., Kimura, R., Okuno, J., Moriwaki, K., Miura, H., Maemoku, H., 2000. Late Pleistocene and Holocene melting history of the Antarctic ice sheet derived from sea-level variations. Mar. Geol. 167, 85–103.
Nakada, M., Lambeck, K., 1987. Glacial rebound and relative sea-level variations: a new appraisal. Geophys. J. Roy. Astronom. Soc. 90, 171–224.
National Institute of Polar Research, 1997. Snow Accumulation. Antarctica: East Queen Maud Land Enderby Land Glaciological Folio. National Institute of Polar Research, Tokyo. Sheet 3.
Nishiizumi, K., Caffee, M.W., Finkel, R.C., 1998. Surface exposure ages and erosion rates of bedrock from Sør Rondane and near Syowa Station, Antarctica. Proc. NIPR Symp. Antarct. Geosci. 18, 62–63.
Nishiizumi, K., Kohl, C.P., Arnold, J.R., Klein, J., Fink, D., Middleton, R., 1991. Cosmic ray produced ^{10}Be and ^{26}Al in Antarctic rocks: exposure and erosion history. Earth Planet. Sci. Lett. 104, 440–454.
Pavlis, N.K., Holmes, S.A., Kenyon, S.C., Factor, J.K., 2012. The development and evaluation of the Earth Gravitational Model 2008 (EGM2008). J. Geophys. Res. 117, B04406 http://dx.doi.org/10.1029/2011JB008916.
Peltier, W., 2004. Global glacial isostasy and the surface of the ice-age Earth: the ICE-5G (VM2) model and GRACE. Annu. Rev. Earth Planet. Sci. 32, 111–149.
Peltier, W.R., 2005. On the hemispheric origins of meltwater pulse 1a. Quat. Sci. Rev. 24, 1655–1671.
Pollard, D., DeConto, R.M., 2009. Modelling West Antarctic ice sheet growth and collapse through the past five million years. Nature 458, 329–332.
Rood, D.H., Brown, T.A., Finkel, R.C., Guilderson, T.P., 2013. Poisson and non-Poisson uncertainty estimations of ^{10}Be/^{9}Be measurements at LLNL–CAMS. Nucl. Instrum. Methods Phys. Res. B: Beam Interact. Mater. Atoms 294, 426–429. http://dx.doi.org/10.1016/j.nimb.2012.08.039.
Shiraishi, K., Dunkley, D.J., Hokada, T., Fanning, C.M., Kagami, H., Hamamoto, T., 2008. Geochronological constraints on the Late Proterozoic to Cambrian crustal evolution of eastern Dronning Maud Land, East Antarctica: a synthesis of SHRIMP U-Pb age and Nd model age data. In: Satish-Kumar, M., Motoyoshi, Y., Osanai, Y., Hiroi, Y., Shiraishi, K. (Eds.), Geodynamic Evolution of East Antarctica: A Key to the East-West Gondwana Connection, Geological Society, London, Special Publications, vol. 308, pp. 21–67.
Shiraishi, K., Osanai, Y., Ishizuka, H., Asami, M., 1997. Geological Map of the Sør Rondane Mountains, Antarctica. Antarctic Geological Map Series, Sheet 35, Scale 1:250000. National Institute of Polar Research, Tokyo.
Staiger, J.W., Marchant, D.R., Schaefer, J.M., Oberholzer, P., Johnson, J.V., Lewis, A.R., Swanger, K.M., 2006. Plio-Pleistocene history of Ferrar Glacier, Antarctica: implications for climate and ice sheet stability. Earth Planet. Sci. Lett. 243, 489–503.
Stone, J.O., 2000. Air pressure and cosmogenic isotope production. J. Geophys. Res. 105, 23753–23759.
Stone, J.O., Balco, G.A., Sugden, D.E., Caffee, M.W., Sass Iii, L.C., Cowdery, S.G., Siddoway, C., 2003. Holocene deglaciation of Marie Byrd Land, West Antarctica. Science 299, 99–102.
Strasky, S., Di Nicola, L., Baroni, C., Salvatore, M.C., Baur, H., Kubik, P.W., Schlüchter, C., Wieler, R., 2009. Surface exposure ages imply multiple low-amplitude Pleistocene variations in East Antarctic Ice Sheet, Ricker Hills, Victoria Land. Antarct. Sci. 21, 59–69.
Suganuma, Y., Miura, H., Okuno, J., 2012. A new sampling technique for surface exposure dating using a portable electric rock cutter. Antarct. Rec. 56, 85–90.
Summerfield, M.A., Sugden, D.E., Denton, G.H., Marchant, D.R., Cockburn, H.A.P., Stuart, F.M., 1999. Cosmogenic isotope data support previous evidence of extremely low rates of denudation in the Dry Valleys region, southern Victoria Land, Antarctica. In: Smith, B.J., Whalley, W.B., Warke, P.A. (Eds.), Uplift, Erosion and Stability: Perspectives on Long-term Landscape Development, Geological Society, London, Special Publications, vol. 162, pp. 255–267.
Takahashi, S., Endoh, T., Azuma, N., Meshida, S., 1992. Bare ice fields in the inland part of Antarctica. Proc. NIPR Symp. Polar Meteorol. Glaciol. 5, 128–139.
Van Autenboer, T., 1964. The geomorphology and glacial geology of the Sør Rondane, Dronning Maud Land. In: Adie, R.J. (Ed.), Antarctic Geology. North-Holland Publishing Company, Amsterdam, pp. 81–103.
White, D.A., Bennike, O., Berg, S., Harley, S.L., Fink, D., Kiernan, K., McConnell, A., Wagner, B., 2009. Geomorphology and glacial history of Rauer Group, East Antarctica. Quat. Res. 72, 80–90.
White, D.A., Fink, D., Gore, D.B., 2011. Cosmogenic nuclide evidence for enhanced sensitivity of an East Antarctic ice stream to change during the last deglaciation. Geology 39, 23–26.
Whitehouse, P.L., Bentley, M.J., Milne, G.A., King, M.A., Thomas, I.D., 2012. A new glacial isostatic adjustment model for Antarctica: calibrated and tested using observations of relative sea-level change and present-day uplift rates. Geophys. J. Int. 190, 1464–1482.
Yamane, M., Yokoyama, Y., Miura, H., Maemoku, H., Iwasaki, S., Matsuzaki, H., 2011. The last deglacial history of Lützow-Holm Bay, East Antarctica. J. Quat. Sci. 26, 3–6.